Catalytic Routes for Direct Methane Conversion to Hydrocarbons and Hydrogen: Current State and Opportunities

Hugo Cruchade, Izabel Medeiros-Costa, Nikolai Nesterenko, Jean-Pierre Gilson, Ludovic Pinard, Antoine Beuque, Svetlana Mintova

Catalytic Routes for Direct Methane Conversion to Hydrocarbons and Hydrogen: Current State and Opportunities

Hugo Cruchade[a,+] Izabel C. Medeiros-Costa[b,+] Nikolai Nesterenko[b,*] Jean-Pierre Gilson[a], Ludovic Pinard[a], Antoine Beuque,[c] Svetlana Mintova[a,*]

[a]Normandie Université, ENSICAEN, UNICAEN, CNRS, Laboratoire Catalyse et Spectrochimie (LCS), 14050 Caen, France.

[b]Total Research and Technology, Feluy, B-7181 Seneffe, Belgium.

[c]Institut de Chimie des Milieux et Matériaux de Poitiers (ICM2P), UMR 7285 CNRS, Poitiers, France.

+ Equally contributed.

ABSTRACT. Natural gas is the cleanest fossil fuel and an abundant source of methane expecting to play an increasingly important role in powering the world's economic growth over the coming decades. Methane has the potential to be a CO_2-free feedstock to co-generate hydrogen (H_2) and added value "building-blocks" chemicals (e.g. olefins and aromatics) for petrochemistry. In this review, the two main processes (i) the oxidative coupling of methane (OCM) for production of ethylene and (ii) the non-oxidative methane dehydroaromatization (MDA) producing hydrogen and benzene have been revealed. Both routes offer direct conversion of methane into final products of interest representing advantages over the several-steps syngas route. The performance of variety of catalysts reported during the last 25 years for OCM (MnNaW, La_2O_3, Li-MgO, etc.) and MDA (M/HZSM 5, M/TNU-9, M/IM-5,

M/ITQ-2, M@SiO_2, M@CeO_2, TaH/SiO_2, GaN/SBA15, single-site M@HZSM-5, bimetallic M-M'/HZSM-5, core-shell structures, M/$Zr(SO_4)_2$ with M=Mo, Fe, Pt) reactions at similar reaction conditions has been compared. The major drawbacks and the novel strategies used to mitigate or even overcome the main challenges related with the performance of the catalysts in both OCM and MDA reactions were critically revealed. For instance, the overoxidation issue in the OCM mitigated by looking at the operating conditions, the use of alternative oxidants, and the application of membrane reactor technology have been disclosed. Concerning the MDA reaction, the major issues related with the deactivation of the catalyst through coke formation or migration and sintering of metallic active phases have been addressed. Strategies for novel robust catalysts, new methods for mild coke removal, pre-treatment under reductive atmosphere were presented. Approaches to improve aromatics yields over coke production by addition of promoters or co-feed reactants to the MDA catalysts have been discussed.

Table of contents

1. Introduction: from low-carbon to zero-carbon future 4
2. Oxidative coupling of methane (OCM) 5
2.1. Overview of OCM and advances in catalysts engineering 5
2.2. Optimal operating conditions for OCM reaction 12
2.3. Alternatives for controlling deep oxidation in OCM process 15
2.4. Outlook for the OCM industrial scenario 18
3. Methane dehydroaromatization (MDA) 19
3.1. Overview of MDA: main drawbacks and new trends in catalysts design 19
3.2. Deactivation of MDA catalyst and mitigation strategies 29
3.2.1. Modes of MDA catalysts deactivation 29
3.2.1.1. Reversible coke formation in MDA catalysts 29
3.2.1.2. Irreversible structural damages of MDA catalysts 34
3.2.2. Evolution of the catalyst stability during the MDA 35
3.2.2.1. Impact of the catalyst pretreatment 35
3.2.2.2. Impact of the reaction conditions 36
3.2.2.3. Impact of the regeneration steps 37
3.3. Improving aromatic production in the MDA 39

3.3.1. Addition of promoters 39
3.3.2. Addition of co-feed reactant 42
3.3.2.1. Addition of H_2 co-feed reactant 42
3.3.2.2. Addition of CO co-feed reactant 44
3.3.2.3. Addition of CO_2 co-feed reactant 45
3.3.2.4. Addition of H_2O co-feed reactant 46
4. Outlook 48
5. References 51

1. Introduction: from low-carbon to zero-carbon future

Most of the methane produced in the upstream and downstream industries is flared leading to non-negligible emissions of CO_2 to the atmosphere. In 2020, the total amount of natural gas flared in the world was almost equivalent to the demand of Central and South America combined.[1] In addition to the methane that is wasted/flared, there are vast natural gas deposits, making methane an abundant source of hydrocarbons in the world.[2] The use of methane as a raw material to produce high value-added chemicals is therefore an alternative that deserves to be highlighted in the current scenario, which seeks to reduce CO_2 emissions and transform the industry through cleaner fossil sources. In this context, the use of methane is certainly part of the solutions that must be implemented in order to achieve net zero emissions by 2050.

Ethylene, hydrogen, and aromatics are some of the most important chemicals that can be produced from methane. The direct production of such molecules from methane transformation is possible via the catalytic oxidative coupling of methane (OCM) and methane dehydroaromatization (MDA) under non-oxidative conditions, avoiding indirect routes such as syngas production.[3–27] Throughout this review these two alternatives for methane conversion will be addressed. The main obstacles faced during the oxidative coupling and dehydroaromatization of methane will be also revealed. Low yields, catalyst stability and coke formation are among the most significant challenges that can affect such processes. Different alternatives aiming to address the above issues are pointed out throughout this review.

In the case of the OCM reaction, the nature of the catalysts and the characteristics of the supports used have shown to have a significant impact on the reaction's performance.[28–32] In addition, the impact of several parameters such as temperature, space velocity, dilution and others will be addressed, and preferable conditions favoring the OCM will be revealed. Furthermore, the CH_4/O_2 ratio appears as a highly important parameter directly affecting conversion, C2 and COx selectivities. The more oxygen fed into the reactor, the more exothermic the process becomes and the more overoxidation occurred thus making it difficult to maintain adequate selectivities to C2 products.[33,34] Other possibilities available for better control of oxidation and heat management such as the use of alternative oxidants (N_2O, CO_2, S_2) and the use of membrane reactors have been also considered.[35–40] An overview of oxidative coupling of methane in the industrial scenario will be provided in this review paper.

In the case of MDA reaction, catalyst's lifetime is a major concern, mainly due to the formation of coke and inactive species responsible for catalyst deactivation.[8,18] Therefore, a special attention is devoted to the nature of coke produced during the MDA and various strategies on the catalyst design avoiding metal migration and enhancing catalysts resilience have been considered. An optimum metal content and novel approaches to incorporate metals in the zeolitic matrix are among the strategies considered while focusing on MDA. Furthermore, knowing that the production of extensive amount of coke is currently unavoidable, focused efforts to address this issue have been devoted. Possible approaches presented here consist on partial coke removal under soft conditions and use of reductive atmosphere in order to avoid structural damages of the catalyst.[41,42] Pretreatment of the catalyst under reductive atmosphere are also presented as a way to prevent migration of the active metallic sites.[43–46] Finally, strategies to improve benzene yields as the addition of metallic promoters[45,47–49] and mixture of other molecules in the feed have been explored.[50–54] As will be shown in the next sections, the reaction performance of the catalysts can be improved by playing with the thermodynamic equilibrium, resulting in changes in terms of coke reduction and benzene yield variations.

2. Oxidative coupling of methane (OCM)

The oxidative coupling of methane occurs through a mixture of methane and an oxidant, commonly oxygen, at temperatures usually above 500 °C, which varies depending on the type of catalyst used. The most attractive products of OCM are ethylene and ethane, although attaining significant methane conversions while maintaining high selectivity to C2 products is quite challenging. The problem with selectivity arises from the thermodynamics of the reactions involved in the OCM reaction, which favors the formation of overoxidized products as CO_x. In fact, complete and partial oxidation of methane to CO_x as well as the combustion of ethane and ethylene can occur.

2.1. Overview of OCM and advances in catalysts engineering

The oxidative coupling of methane is widely recognized as a mixed catalytic and gas-phase process.[24–27] A generic scheme considering the different pathways of reactants/intermediates

in OCM is presented in **Scheme 1**. The catalyst is initially activated by oxygen present in the feed. Then the methane molecules react with the oxygen on the catalyst surface resulting in the formation of $CH_3^{\bullet}$ radicals. The coupling of such radicals to the formation of ethane takes place in the gas phase and the production of ethylene is achieved by subsequent dehydrogenation of ethane. In turn, the non-selective oxidation reactions leading to the formation of CO_x occur in both the gas-phase and on the catalyst surface. Therefore, the development of catalysts capable of limiting CO_x production (especially CO_2), while promoting the formation of methyl radicals and C2 molecules, would be a key step toward commercializing the OCM process in an economically feasible manner.

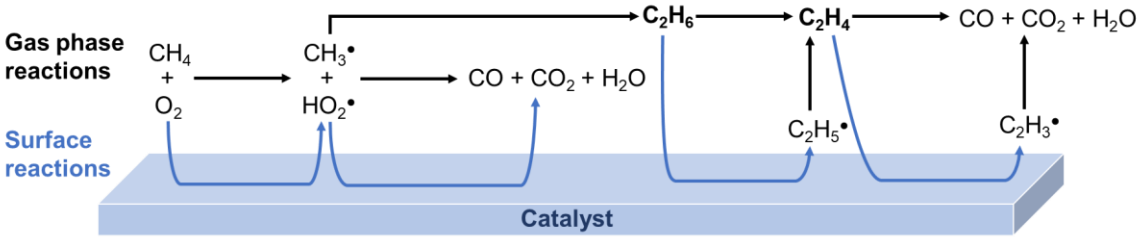

Scheme 1. General mechanism in the oxidative coupling of methane considering the different pathways of reactants/intermediates in gas phase and surface reactions.

Technologies based on the OCM process are not yet commercially viable. However, efforts have been devoted to change this scenario. Siluria Technologies was the first to develop a process on a demonstration scale plant.[55] In their technology, methane and optionally ethane are initially converted into ethylene in a fixed-bed reactor via the OCM process. The reaction yield is increased by adding ethane to the second section of the reactor, where ethane is converted to ethylene through dehydrogenation.[56] Siluria Technologies has also developed nanowire catalysts operating at low temperatures (~500-700 °C), compared to high temperatures commonly applied in the OCM (> 800 °C).[57,58] The catalysts developed by

Siluria are based on Sr doped La_2O_3 nanowire and they are able to convert 14% methane with about 13% selectivity at 650 °C.[57] In a recent study, over 35 different combinations of alkaline earth metals as dopants (D) in D/rare earth oxides catalysts were investigated and Sr doped La_2O_3 was revealed to be the most C2 selective, while undoped La_2O_3 was the most active catalyst.[59] Furthermore, it was observed that excess of Sr in the catalyst generates the formation of secondary phases, primarily amorphous (SrO, $Sr(OH)_2$, SrO_2 and $SrCO_3$) that favors oxygen transport and shows improved selectivity.[59] According to the theoretical predictions based on DFT calculations, the Sr dopant may lead to an increase of the catalytic efficiency of the La_2O_3 catalyst by increasing active oxygen radical sites and enhancing the basicity of the catalyst.[60]

Despite the decent activity and stability of the Sr/La_2O_3 based catalysts, the search for other types of catalysts presenting higher C2 yields has attracted more attention in the field of OCM. Several catalysts were subject to a statistical study in order to understand the implications of their composition on the OCM catalytic performance.[28] Based on the data obtained from the statistical analysis, it has been proposed that their activity can be improved by inserting dopants like W, Mn and Cl into highly basic oxides catalysts such as Mg and La. Moreover, the C2 selectivity was shown to be enhanced by the addition of alkaline and alkaline earth metals.[28] **Figure 1** shows the performances of the common MnNaW, La_2O_3 and Li-MgO based catalysts in comparison to recently explored materials in the OCM process.

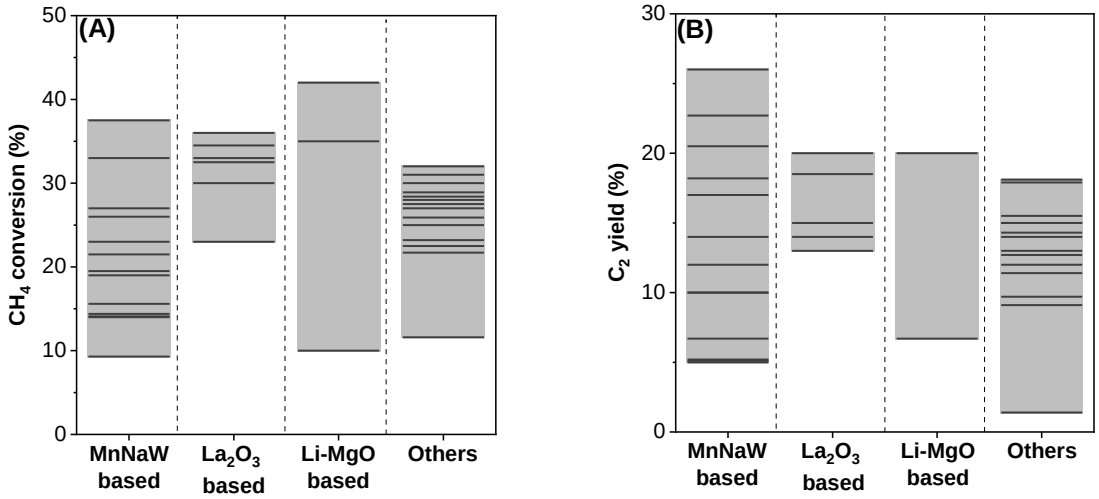

Figure 1. (**A**) CH_4 conversion and (**B**) C_2 yield on different OCM catalysts. Each line corresponds to one datapoint taken from references presented in **Table 1**; the gray columns show the trends.

Table 1. Performances of catalysts and conditions of the OCM reaction reported in the open literature.

Catalyst	**OCM condition**			**Performance**			**Reference**
	Temperature	GHSV	CH_4/O_2	X_{CH_4}	S_{C2}	Y_{C2}	
	°C	$ml_{CH4}\ g_{cat}^{-1}\ h^{-1}$		%	%	%	
MnNaW based catalysts							
$NaCl/Mn_2O_3/SiO_2$	750	3000	4/1	37.5	60.5	22.7	[29]
Mn Na_2WO_4/ZeoA	750	60000	4/1	19.0	55.0	10.0	[30]
MnxOy– Na_2WO_4/SiO_2	750	4200	4/1	19.5	60.0	12.0	[61]
Mn Na_2WO_4/SiO_2	850	2700	4.5/1	33.0	8.00	26.0	[62]
MnxOy– Na_2WO_4/SBA-15	750	72000	4/1	14.0	70.0	10.0	[31]
MnxOy-Na_2WO_4/MCF-17	750	60000	4/1	15.6	33.0	5.0	[63]
Rh-MnxOy- Na_2WO_4/MCF-17	750	60000	4/1	9.3	55.6	5.2	[63]
Ir-MnxOy-Na_2WO_4/MCF-17	750	60000	4/1	14.4	46.7	6.7	[63]
Pt-MnxOy-Na_2WO_4/MCF-17	750	60000	4/1	14.1	36.1	5.1	[63]
Mn_2O_3-$Na_2WO_4/Ce_{0.15}Zr_{0.85}O_2$	700	4000	5/1	26.0	70.0	18.2	[64]
MnOx-Na_2WO_4/TiO_2 MnOx-Na_2WO_4/MgO	700-800	4000	5/1	~23.0	~73 (C2-C3)	~17	[65]
MnOx-Na_2WO_4/SnO_2	740-800	4000	5/1	~21.5	~64(C2-	~14	[65]

$MnOx-Na_2WO_4/ZnO$					C3)		
		8000	5/1	27.0	76.0	20.5	[66]
La_2O_3 based catalysts							
La_2O_3-Li-Mn/ WO_3/TiO2	750	600	2.5/1	~30.0	~60.0	~20.0	[67]
5%Sr/La_2O_3:SiO_2	800	9600	8/1	~33.0	~64.0	~21.1	[32]
2%Sr/La_2O_3:SiO_2	800	9600	8/1	~23.0	~6.05	~15.0	
La_2O_3	800	-	3/1	~32.5	~40.0	~13.0	
0.8% Sr/La_2O_3	800	-	3/1	~34.5	~40.0	~14.0	[68]
12% Sr/La_2O_3	800	-	3/1	~36.0	~47.0	~18.5	
Li-MgO catalysts							
1.1% Li-MgO	750	9000	8/4	10.0	67.0	6.7	
5.5% Li-MgO	750	9000	8/4	35.0	58.0	20.0	[69]
11.2 Li-MgO	750	9000	8/4	42.0	47.0	20.0	
Others							
$ZnO–Sm_2O_3$	775	14400	5/1	21.7	41.9	9.1	
$MgO–Sm_2O_3$	775	14400	5/1	23.2	49.2	11.4	[70]
$CaO–Sm_2O_3$	775	14400	5/1	25.0	57.2	14.3	
$SrO–Sm_2O_3$	775	14400	5/1	25.9	59.8	15.5	
$La_{0.8}Ce_{0.2}O_{1.5+\delta}$	450-500	30000	3/1	~30.0	~45.0	~13	[71]
La_2CeO_7	750	18000	4/1	~27.5	~55.0	~15	[72]
SnO_2	800	18000	4/1	11.6	3.0	1.4	[73]
BaF_2:SnO_2	800	18000	4/1	22.5	26.2	12.7	[73]
$BaCl_2$:SnO_2	800	18000	4/1	28.0	38.3	17.9	[73]
$BaBr_2$:SnO_2	800	18000	4/1	28.9	50.1	18.1	[73]
$BaSnO_3$	800	18000	4/1	28.4	30.3	14.0	[73]
$La_2Li_{0.5}Al_{0.5}O_4$	775	10000	3/1	32.0	47.0	15.0	[74]
$LaAlO_3$	775	10000	3/1	31.0	38.0	12.0	[74]
Ag/SiO_2 + Plasma	400	6000	4/1	27.0	36 (C2+)	9.7	[75]

$MnNaW/SiO_2$ is one of the most studied catalysts and it is also reported as one of the most promising system, due to the high C2 yield and stability on stream.[61,62,76] Serres *et al.* showed that increasing the quantity of active sites in the catalyst contributed to an increase of the catalytic activity up to 19.5% W.[77] However, by extrapolating the concentration of active sites up to 41%, a drop in activity is observed, which was associated with a loss in the

catalysts surface area. Such textural transformation was due to the large amount of Na that promote the formation of low surface area cristobalite phase.[77] Other supports such as SiC and alumina were also tested, but the problem associated with cristobalite formation partially affected the performance of the SiC supported catalysts, while low selectivity was observed when alumina was used as a support. The latter was justified by the low dispersion of active sites on the alumina surface and therefore large extensions of alumina quenching the radicals were observed.[77]

Furthermore, a direct relationships between the activity of catalysts supported on SiC and SiO_2 and the concentration of active sites and specific surface were reported (**Figure 2 A**).[77,78] Likewise, Fleischer *et al.*[79] observed that the increase of the specific area of the catalyst (up to 4 m^2 g^{-1}) is associated with an increase in the activity of the catalyst. Another study also showed that the decrease in the amount of Na_2WO_4 from 7% to 4% contributed to the reduction in the size of catalysts particles having a direct effect on the increase of catalysts activity as shown in **Figure 2 B**.[30] The results summarized in **Figure 2** indicate that the active sites in OCM catalysts must be highly accessible and homogeneously distributed in supports with high specific surface areas. Furthermore, the activity of the catalysts along the reactions is also related to the structural stability of the support.[78]

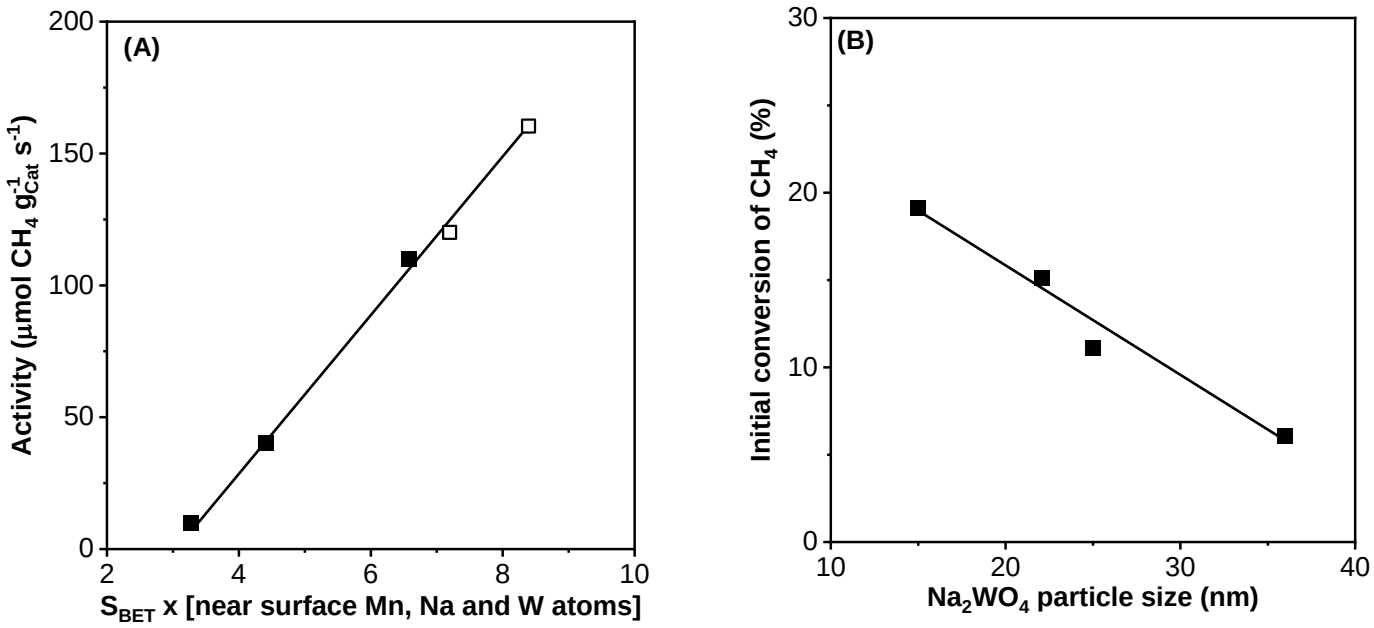

Figure 2. Activity of MnNaW catalysts supported on SiO_2 (■) and SiC (□) as a function of (**A**) the concentration of active phase (Mn, Na, W) (reproduced from Ref[77]) and (**B**) the Na_2WO_4 particle size (reproduced from Ref[30]).

It is well known that silica-based supports (SiO_2) may transform to cristobalite during catalysts preparation in the presence of Na. The cristobalite was reported to be a reason for a better distribution of active phases and formation of more selective Mn_2O_3 species.[80,81] The use of mesoporous silica (SBA-15) as a support showed an improvement in the performance of the Mn-Na-W based catalyst compared to the conventional amorphous SiO_2 support.[82] Methane conversion was improved by a factor of two, with similar C2 selectivity and a considerable increase in the ethylene/ethane fraction, compared to other silicon-based supports was reported. Importantly, all supports including SBA-15 were transformed into cristobalite. The improved performance of the catalyst on the SBA-15 support was then associated with a better distribution and a larger number of active sites, as a result of the high surface area and ordered mesoporous structure.[82] Other supports such as MgO, SrO, ZrO_2, Al_2O_3 and La_2O_3 were also investigated and showed lower performance than the conventional SiO_2 supported catalyst.[81,82] Yildiz *et al.* showed that the use of rutile and anatase (TiO_2) with

Fe_2O_3, Fe_3O_4 and SiC were more performant than the SiO_2-based catalyst, although stability problems have been reported when using anatase.[82] In a more recent study, the use of rutile, mesoporous rutile and anatase showed lower C2 yield compared to the SiO_2 support.[81,83] In addition to the type of the support, the nature of the salts used for the impregnation also seemed to promote a homogeneous distribution of the active phase, contributing to an improvement of the activity. For instance, the Mn acetate showed more encouraging results than the Mn nitrate.[30]

The stability of OCM catalysts is also a challenging issue due to the amount of heat released during the reaction and this needs a special attention. Thermal treatments such as calcination of the catalyst ($MnNaW/SiO_2$) under a specific atmosphere proved to be efficient towards improving the stability. The thermal treatment was found to promote phase change of the silica support to cristobalite and denser phases such as quartz. Therefore, despite the stability gain, a loss of the catalyst specific surface area occured, which leads to a decrease in methane conversion. Best results were obtained when calcination was carried out under inert atmosphere thus favoring the interactions between W and reduced Mn species.[84] On the other hand, in the presence of oxygen during calcination, Mn was found in the form of Mn_2O_3 oxides, which could hinder the performance of the catalyst.[84] Recently, a new approach where SiC particles were incorporated into the SiO_2 matrix of the catalyst through spray drying proved to be an efficient approach towards improvement of catalysts thermal stability. As a result, a novel $MnNaW/SiO_2$-SiC catalyst with higher conversion and selectivity over time on stream compared to the traditional catalyst based on SiO_2 support was disclosed.[85]

2.2. Optimal operating conditions for OCM reaction

The thermal effects taking place during the OCM reaction can be altered by varying some operational parameters including temperature, space velocity, dilution with inert gas, methane to oxygen ratio, etc. Since the heat generated during the OCM reaction can affect its

performance, experimental settings in which the surface and gas phase reactions are balanced have to be established. In this way, the optimum conditions toward enhance conversion while retaining strong C2 selectivity and preventing product overoxidation have to be defined. One strategy is to enhance exothermic methyl radical coupling in order to create ethane, while favoring endothermic ethane dehydrogenation to obtain large ethylene fractions, all while avoiding product overoxidation. Recently M. Kim *et al.*[33] investigated the catalytic activity of Mn-Na_2WO_4/SiO_2 in OCM reaction under varying the quantity of catalyst (0.5-1.5 g), temperature (750-875 °C), dilution with inert gas (0-75%), GHSV (9600-19200 $cm^3\ g^{-1}\ h^{-1}$) and methane to oxygen ratio (2-4). In certain conditions, further increase of the quantity of catalyst more than 1 g proved to be difficult in terms of controlling the reaction temperature or pressure rise. This issue is quite challenging when aiming extending the process to industrial scale. Among the parameters investigated, it was observed that the increase of temperature directly favors higher methane conversion and ethylene/ethane ratio. Dilution rate with inert gas (N_2) between 25-75% promotes a decrease in the reaction temperature and consequently lower the methane conversion and ethylene/ethane ratios. A similar response was obtained when GHSV is increased and consequently the residence time inside the reactor was reduced. In the case of less diluted systems (N_2 of up to 25%), an increase in the gas phase reactions such as dehydrogenation of ethane and formation of CO with an unfavorable balance to C2 selectivity was observed. On the other hand, increasing the methane to oxygen ratio promoted the C2 selectivity, though the conversion is reduced, as the latter is limited by the reaction stoichiometry and therefore by the amount of oxygen supplied as the limiting reactant.[33] For example, keeping the flow rate, temperature and dilution constant, the methane conversion and C2 selectivity changed from 30% and 66% to 45% and 44%, for the CH_4/O_2 ratio of 4 and 2, respectively. Although in this case the yields were similar around 20%, an almost two times higher ethylene/ethane ratio and higher production of CO and CO_2 were

obtained by the CH_4/O_2 ratio of 2.[33] Importantly, due to the danger of explosion, the ratio methane/oxygen must be carefully examined before any test.[86]

Similar conclusions were made for La_2O_3-CeO_2 and LaSr/CaO catalysts.[34,87] In that case, the parameters such as flow velocity and methane to oxygen ratio were investigated. It was demonstrated that the higher the methane to oxygen ratio, the higher the C2 selectivity was obtained, but the lower the methane conversion.[34,87] It is also interesting to mention that for higher methane to oxygen ratios, the ignition temperature was also higher.[87] Furthermore, by decreasing flow velocities in the range 5-40 ms at the same feed temperature, a positive effect on simultaneous methane conversion and C2 selectivity was observed.[87] For the same catalytic system, the effect of the feed dilution with 55% N_2, proved to be beneficial for increasing the yield of the C2 fraction.[88] The use of a diluent (N_2) had a direct effect on the oxygen dilution leading to an increase in methane conversion. The methane coupling process was enhanced by such dilution, whereas the competing deep oxidation reactions were inhibited. However, it was observed that higher dilutions would also cause disadvantages for the methane coupling, as the reaction yield decreases.[88]

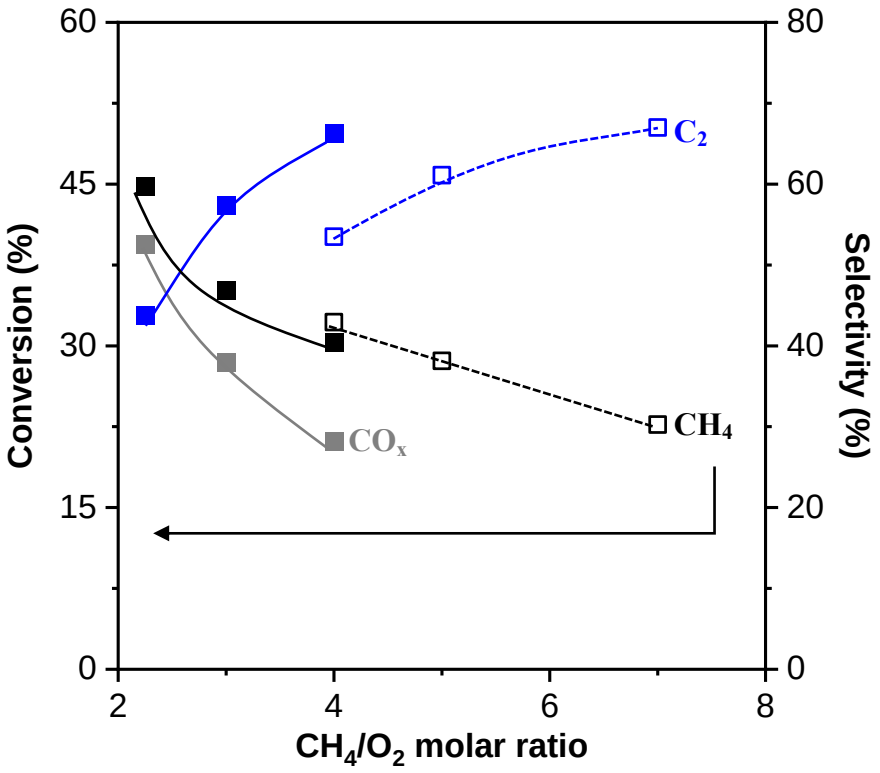

Figure 3. Effect of CH_4/O_2 ratio on the conversion and selectivity of oxidative coupling of methane in the presence of Mn-Na_2WO_4/SiO_2[33] (■) and La_2O_3-CeO_2[34] (□) catalysts.

The use of GHSVs between 8000 and 12000 h^{-1} were identified as the best conditions for a perovskite-type catalyst in the OCM process.[89] The C2 yield decreased with further increase of the GHSV. Considering the CH_4/O_2 ratio, values between 1-3 showed decent C2 yields, and the ideal condition at CH_4/O_2 =2 and 12000 h^{-1}, where an ethylene yield of about 19% was obtained (C2 yields of 23.9%) was identified.[89]

2.3. Alternatives for controlling deep oxidation in OCM process

Recently the use of alternative oxidants for the OCM process was reviewed by Arinaga *et al.*[38]. N_2O, CO_2 and S_2 were identified as promising candidates for use as mild oxidants in the OCM. The replacement of O_2, in addition to promoting the reuse of waste resources, was also

reported to have a positive effect on the safety of the process, as the risk of explosion can be minimized. Although the conversion decreased when N_2O was used instead of oxygen, it has been reported that using N_2O results in better C2 selectivity. As an example, when oxygen was substituted by N_2O as the oxidant, selectivity to C2 was increased in the case of Li/CaO, Li/MgO, RbWSi and NaWSi based catalysts.[35–37] Considering the last catalyst, an improvement from 14% to 83% in C2 selectivity was reported when N_2O was used.[35] The high selectivity obtained in the presence of N_2O are most likely due to the fact that such molecules generate different oxygen species that are more selective to C2.[35,36]

Analogous to N_2O, CO_2 also produces oxygen species that affect the methane oxidation. Experimental work indicated that CO_2 decomposes and forms CO and O* species promoting up to 94% C2 selectivity when applied together with the $MnNaW/SiO_2$ catalyst. While the methane conversion of about 5% was obtained in this system.[90] Other challenges were reported using CO_2 in OCM such as primarily acetylene formation[91] and a competition with the dry reforming reaction.[92] In turn, co-feeding of CO_2 in the presence of O_2 was also investigated and indicated slight improvement of the catalyst activity.[93]

Disulfur (S_2) is another oxidant that can be used to replace O_2 in the OCM reaction. S_2 can react with methane and form a mixture of H_2S and ethane or ethylene, through the coupling mechanism.[94] Despite the endothermic process, methyl mercaptans can also be formed. Furthermore, total oxidation of methane with S_2 resulted in the formation of CS_2, which is similar to the production of CO_2 with O_2. Thermodynamically, the formation of CO_2 during the conventional OCM is much more favorable than the formation of CS_2 using the S_2-OCM catalyst.[94] The oxidation of methane with S_2 is less exothermic and by-products of the reaction such as H_2S and C_2S can be used as raw material in the Claus process[95] and as a solvent[96], respectively. Several unsupported metal sulfides including MoS_2, RuS_2, TiS_2 and PdS showed improved activity in the S_2-OCM catalyst.[94] It was shown that the weak M–S

bonds are more reactive and can easily activate C–H bond in methane and further form CH_x intermediates, leading to overoxidation and production of CS_2. As a result, even though their activity is lower, catalysts with stronger M-S bonds have the advantage of being more selective. Furthermore, the dispersion of the metal sulfide over a support showed an improve performance of the S_2-OCM catalyst. The catalyst prepared by 10% palladium sulfide supported on ZrO_2 displayed a methane conversion of about 16% and ethylene selectivity of almost 17% at 1050 °C.[94]

The use of membranes represents another alternative to control high oxygen partial pressure and consequently the formation of oxidation products as CO_x. Thus, the primary benefit of a membrane reactor is to provide effective oxygen distribution resulting in low oxygen partial pressure all along the reactor, favoring selectivity to C2 products and significantly improving of methane conversion.[97] Furthermore, the inclusion of a membrane in the reactor resulted in better heat distribution and minimize hot spots that might arise as a result of the OCM reaction's exothermicity.[97] A techno-economic assessment analysis exploring the integration of membrane reactors on the OCM process was performed, indicating that the use of membranes promote a reduction of cost of ethylene production (595-695 € t^{-1} ethylene) with 25%-30%, when compared to naphtha steam cracking.[98] In general, the promising effect of using membranes in the OCM process motivated the researchers to explore further various possibilities.[39,40] Dense and porous membranes were proposed for application in OCM. Both technologies ensure homogeneous distribution of oxygen throughout the reactor, however, dense membranes allowed for selective oxygen species permeation, which was not feasible with porous membranes.[99] Another disadvantage of the porous membrane is the risk of back-permeation, which can have serious consequences on the performance and safety of the process.[39,99] Oxygen ionic conducting (OIC) and mixed oxygen ionic and electronic conducting (MIEC) membranes as dense membranes were

explored in the OCM.[100] Such membranes present the benefit of promoting the transport of oxygen ions that are more selective to the formation of ethylene, avoiding the products of overoxidation.[100] Ionic membranes were also applied in electrochemical reactors, which have the possibility to tune the oxygen permeability by altering the electric current.

Although the use of membranes have shown to be very promising, some challenges still need to be considered. The reduction in permeability of dense membranes due to the high temperatures of the process, the need for a large amount of membranes to supply the entire demand for oxygen, and back-permeation in the porous membrane, as already mentioned have to be further consided.[99,100,101] The interactions of the catalyst with the membrane has to be also considered, since it can lead to the formation of different phases that can hinder the permeation in the membrane.[102]

2.4. Outlook for the OCM industrial scenario

The Siluria's oxidative coupling of methane technology with a commercial demonstration plant in La Porte, Texas was developed in 2019. Nowadays, Siluria's technology is used to convert natural gas to fuels and chemicals by Lummus.[103] As mentioned earlier, the technology is based on a post-bed ethane cracking zone, in order to guarantee higher ethylene yields.[56] Although it is an interesting alternative, the technology requires the introduction of ethane for the process. The intellectual property as well as facilities of this technology belonged to the McDermott.[104]

One of the biggest obstacle for the commercialization of the OCM technology is linked to the "conversion or selectivity" dilemma and the challenges that prevent increasing the C2 yield of the reaction. To overcome these limitations, strategies linked to the OCM technology are emerging combining valorization of other products formed during the reaction.

In a recent patent from Sabic Technologies, a process combining two different reaction zones of oxidative coupling of methane and partial oxidation of methane was proposed.[105]

The idea was to take advantage of the effluent produced through the OCM in the second reaction zone of catalytic partial oxidation to produce mainly C2 and synthesis gas (CO and H_2) in addition to side products such as H_2O and CO_2.[105] Besides, the ongoing European project C123 also addressed the concept of atomic economics for the production of ethylene from methane.[106] In this case, the oxidative conversion of methane (OCoM) produces initially (ideally) C2, CO and H_2 through a combination of OCM and dry reforming of methane (DRM) reactions among others in the same step.[106] The advantage behind the C123 strategy is the direct use of the effluent from the OCM reactor (C2, CO and H_2) in the hydroformylation reactor to generate high value C3 products (propylene) by dehydration. Very importantly, this process will relay on exploiting pristine or wasted sources of methane as well as biogas containing CO_2.[106]

3. Methane dehydroaromatization (MDA)

3.1. Overview of MDA: main drawbacks and new trends in catalysts design

The catalytic upgrading of methane under non-oxidative conditions is an attractive way to produce directly valuable hydrocarbons. Methane is reacted with a catalyst to produce selectively benzene as well as dihydrogen through the methane dehydroaromatization reaction, according to the following equation:

$$6CH_{4(g)} \rightleftarrows C_6H_{6(g)} + 9H_{2(g)} \quad \textbf{(1)}$$

The high potential offered by MDA reaction to produce valuable hydrocarbons and energetical resources has received significant attention from researchers during the past decades. Various catalytic systems have been reported and discussed in details in many review papers.[3–22]

In the current review we summarized the best results obtained with different catalytic systems reported during the last 25 years regarding the methane conversion, C_2 products and

benzene yields, as well as the used operating conditions (**Figure 4** and **Table 2**). As can be seen from **Table 2**, the Mo/HZSM-5 is the most investigated catalyst for the MDA reaction since the very first report in 1993.[107] Usually, the MDA reaction is carried out at temperatures from 650 to 800 °C, leading to an average benzene selectivity of 70%.[41,43,108–118] Other catalysts for the MDA with lower performance including Fe/HZSM-5, GaN/SBA-15, TaH/SiO_2 and bimetallic Pt-X/HZSM-5 have been reported. On the contrary, highly dispersed $Fe@SiO_2$[119,120] and $Pt@CeO_2$[121] showed high benzene and C_2 production during tens of hours of reaction. However, both catalysts showed some disadvantages as high reaction temperature (≥ 950 °C) and high methane dilution for the $Pt@CeO_2$ (1 vol % CH_4 in He). The high selectivity to benzene (22%) and ethylene (55%) on the $Fe@SiO_2$ catalyst at a methane conversion of 32% at 1020 °C is diverged with the radical mechanism proposed.[119,122,123] It is important to note that the potential development of MDA using the $Fe@SiO_2$ catalyst will require an appropriate design of the process as a whole, and more precisely a reactor to control the non-selective gas-phase reactions should be considered.

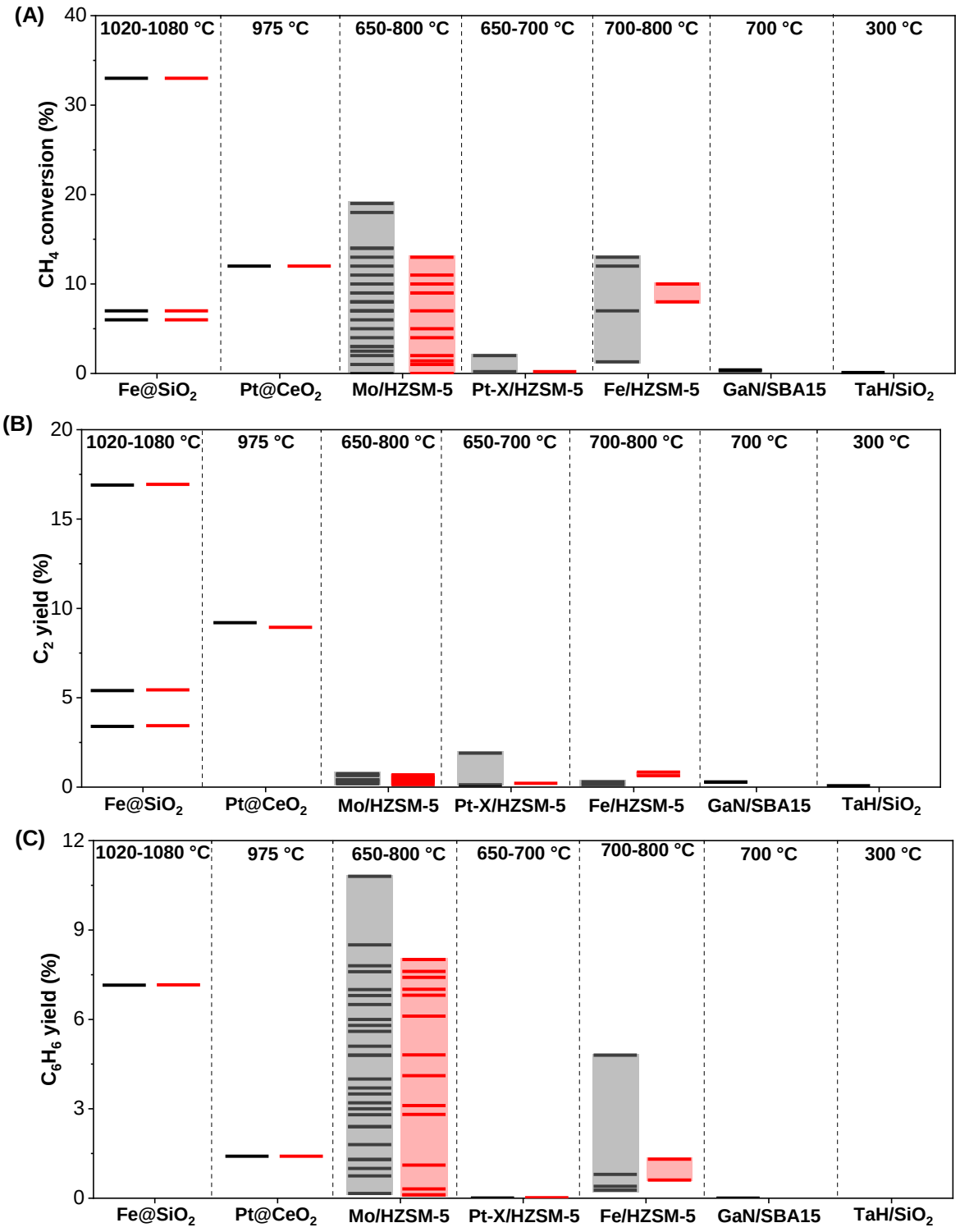

Figure 4. (**A**) Conversion of methane, (**B**) yield of C_2 products and (**C**) yield of benzene using different catalytic systems reported in the literature at TOS of 250-300 min (dark) and 600 min (red). Each line corresponds to one value taken from **Table 2;** the columns in gray and red show the trends.

Table 2. Performance of catalysts and conditions for MDA reaction reported during the last 25 years.

Catalyst	MDA conditions				Performance																Ref
					TOS 100 min					250-300 min					600 min						
Metal (wt %); method of metal incorporation; Si/Al	T, P[1]	GHSV	Feed composition	Pretreatment	X_{CH_4}	$Y_{C_6H_6}$	Y_{Aro}	Y_{C_2}	Y_{Coke}	X_{CH_4}	$Y_{C_6H_6}$	Y_{Aro}	Y_{C_2}	Y_{Coke}	X_{CH_4}	$Y_{C_6H_6}$	Y_{Aro}	Y_{C_2}	Y_{Coke}		
	°C, bar	$ml_{CH4}\ g_{cat}^{-1}\ h^{-1}$	vol %		/%	/%	/%	/%	/%	/%	/%	/%	/%	/%	/%	/%	/%	/%	/%		
Fe/HZSM-5 catalysts																					
2-4; WI; 15	750	1620	CH_4/N_2-90/10	Δ: Ar	6-7	0	/	0.1	/	7	< 1	/	0.3	/	8	0.6-1.3	/	0.7	/		[124]
6; WI; 25	750	1350	CH_4/Ar-90/10	Δ: CH_4/Ar/He-43/5/52	14.2	0.2	/	/	14	12	4.8	/	0.3	6.9	/	/	/	/	/		[125]
2; IE; 12.5	800	1500	CH_4/N_2-95/5	Δ: Ar	15.0	/	11	/	/	11.5	/	4	/	/	/	/	/	/	/		[126]
1; WI; 40	700	3750	CH_4/He-50/50	Δ: He	0.7	< 0.1	/	0.4	/	1.3	0.3	/	0.1	/	/	/	/	/	/		[127]
2-Fe-0.5-Au; WI; 15	750	3000	CH_4/Ar-67/33	/	13.0	/	3	/	/	12.6	/	2.4	/	/	9.7	/	1.5	/	/		[128]
Fe@SiO_2 catalysts																					
/; MF	1020	/	CH_4/Ar-90/10	Δ: He	6.0	/	2.0	3.0	0	7.0	/	2.3	3.4	0	6.8	/	2.3	3.4	0		[129]
	1080	8000	CH_4/H_2/Ar-40/50/10	Δ: He	6.2	/	0.6	5.4	0	6.2	/	0.6	5.4	0	6.2	/	0.6	5.4	0		
0.5; MF	1020	14500	CH_4/N_2-90/10	Δ: CH_4/N_2-90/10	33.0	7.2	/	17	0	33.0	7.2	/	17	0	33.0	7.2	/	17	0		[119]
Pt@CeO_2 catalysts																					
0.5; /	975	6000	CH_4/He-1/99	Δ: He	12.0	1.5	/	9.0	0	12.0	1.4	/	9.2	0	12.0	1.4	/	8.9	0		[121]
GaN/SBA15 catalysts																					
15; WI	700	2400	CH_4/Ar-80/20	Δ: Ar	0.4	< 0.1	/	0.3	/	0.3	< 0.1	/	0.3	/	/	/	/	/	/		[130]
11; WI	700	2200	CH_4/Ar-80/20	Δ: Ar	0.4	< 0.1	/	0.3	/	0.4	< 0.1	/	0.3	/	/	/	/	/	/		[131]
TaH/SiO_2 catalysts																					

/	300, 50	616	CH_4	/	/	/	/	/	/	0.1	/	/	0.1	/	/	/	/	/	/	[132]
Bimetallic Pt-X/HZSM-5 catalysts																					
1Pt-0.8Bi; WI; 40	650	4481	CH_4-10%	400 °C (4 h) under H_2/N_2 - 30/70	2.1	/	/	1.9	/	2.1	/	/	1.9	/	/	/	/	/	/	[133]
0.6Pt-0.7Sn; WI; 40	700	2520	CH_4	Reduction from roomT to 500 °C then Δ: He	0.1	< 0.1	/	0.1	/	0.2	< 0.1	/	0.1	/	0.2	< 0.1	/	0.2	/	[134]
Bimetallic Mo-X/HZSM-5 catalysts																					
0.5Pt-2Mo; WI; 35	700	1458	CH_4/Ar-90/10	Precarburized at 750 °C (1 h) CH_4/H_2	8.0	6.6	/	/	0.3	7.5	5.8	/	/	0.6	/	/	/	/	/	[47]
0.6Co-6Mo; WI; 15	700	1365	CH_4/N_2-91/9	Δ: CH_4/H_2 - 10/90	/	6.7	/	/	/	/	7.0	/	/	/	/	7.0	/	/	/	[45]
0.6-1Ni-6Mo; WI; 15	700	1500	CH_4/N_2-91/9	Δ: CH_4/H_2 - 10/90	/	6.5	/	/	/	/	6.5	/	/	/	/	6.1	/	/	/	
0.2Fe-6Mo; WI; 15	700	1365	CH_4/N_2-91/9	Δ: CH_4/H_2 - 10/90	/	5.5	/	0.2	/	/	6.8	/	0.3	/	/	6.8	/	0.3	/	[49]
1Re-4Mo; WI; 23	700	2550	CH_4/N_2-85/15	Δ: CH_4/N_2-85/15	/	2.0	3.0	0.6	/	/	1.3	1.8	0.7	/	/	1.1	1.3	0.7	/	[135]
0.7NiO + [12Mo/HZSM-5; WI; 11.5]; PM	700	2700	CH_4/He-90/10	Δ: CH_4/He/Ar-45/5/50	11.0	/	5.0	/	/	9.0	/	5.5	/	/	/	/	/	/	/	[136]
3Zn-3Mo; WI; 25	700	1443	Natural gas (96.2%CH_4-2.3%Ethane-1.5%C2-C3)	Δ: N_2	5.0	4.0	/	/	1.5	8.0	3.2	/	/	1.2	/	/	/	/	/	[137]
0.5Pt-0.5Sn-2Mo; WI; 35	700	1460	CH_4/Ar-90/10	At 700 °C (1 h) under N_2	7.8	/	6.0	/	/	6.8	/	5.0	/	/	/	/	/	/	/	[138]

Mo/HZSM-5 catalysts

6; MM; 25	700	1443	Natural gas (96.2%CH_4-2.3%Ethane-1.5%C2-C3)	Δ: N_2	/	4.0	5.5	0.3	/	/	3.5	4.7	0.8	/	/	/	/	/	/	[139]
6; WI; 25	700	1443	Natural gas (96.2%CH_4-2.3%Ethane-1.5%C2-C3)	Δ: N_2	11.0	3.5	/	/	3.5	14.0	3.0	/	/	6.6	/	/	/	/	/	[137]
6; MM; 10	700	1400	CH_4/N_2-80/20	Δ: N2 to 650 °C then Δ: CH_4/N_2-80/20	9.8	6.2	7.8	0.2	1.6	7.0	4.8	5.8	0.4	0.8	4.0	2.8	3.4	0.5	0.1	[108]
5; WI; 15	700	2400	CH_4/N_2-0.66/0.34	Δ: He	7.5	4.8	/	/	/	5.5	4.0	/	/	/	5.0	3.1	/	/	/	[109]
10; WI; 10	700	1550	CH_4/N_2-91/9	Δ: H_2	12.5	7.1	/	0.2	4.5	10.0	7.8	/	0.2	1.1	9.0	7.4	/	0.2	0.2	[110]
16; WI; 25	700	1350	CH_4/Ar-90/10	Δ: CH_4/Ar/He-45/5/50	13.8	/	11	0.3	/	12.5	/	10.5	0.4	/	11.0	/	10	0.5	/	[46]
4; WI (silylated); 20	700	1710	CH_4/N_2-95/5	Δ: He	9.0	6.9	/	0.3	0.9	4.5	2.8	/	0.7	0.1	1.4	0.3	/	0.5	0.2	[111]
6; WI (silylated); 15)	700	1710	CH_4/N_2-95/5	Δ: CH_4/He-80/20	8.0	5.6	/	0.4	1.4	2.5	1.3	/	0.7	0.3	1.0	0.1	/	0.1	0.8	[118]
5; WI; 13	700	2850	CH_4/N_2-95/5	/	6.0	5.0	/	/	/	3.0	1.8	/	/	/	/	/	/	/	/	[112]
2; WI; 30	700	0	CH_4/N_2-95/5	Δ: CH_4/N_2	/	3.0	/	/	/	/	/	/	/	/	/	/	/	/	/	[140]
5; /; /	650	0	CH_4/N_2-95/5	Δ: CH_4/N_2-95/5	3.5	1.7	/	0.4	/	1.6	0.8	/	0.4	/	/	/	/	/	/	[141]
10; WI; 15	700	1550	CH_4/N_2-91/9	Δ: H_2 then CH_4 (20 min) at 700 °C then cooling and Δ: He	12.8	8.0	/	/	/	10.5	8.5	/	/	/	9.5	8.0	/	/	/	[43]
10; WI; 15	750	0	0	/	12.0	7.7	/	0.2	3.7	19.0	6.0	/	0.2	12.8	/	/	/	/	/	[113]

2.5; WI; 20	700	7200	CH_4/H_2/He-40/1/49	/	/	5.1	/	/	/	/	4.8	/	/	/	/	/	/	/	/	50
4; MM; 15	750	750	CH_4/He-50/50	Calcination at 750 °C then from rT to 750 °C CH_4/H_2-50/50	21.0	12.8	/	/	/	18.0	10.8	/	/	/	/	/	/	/	/	114
4; WI; 15	700	1620	CH_4/N_2-90/10	Δ: Ar	16.0	5.6	/	0.2	/	14.0	5.6	/	0.4	/	13.0	4.8	/	0.5	/	142
2; WI; 20	800	4200	CH_4/CO/Ar-85/5/10	Δ: He to 650 °C, then 650 °C (20 min) Ar/CH_4-10/90 then from 600 to 800 °C -H_2	18.5	12.8	/	/	/	1.2	0.2	/	/	/	/	/	/	/	/	115
2; WI; 13	725	3600	CH_4/N_2-88/12	/	7.3	3.5	/	0.6	/	2.5	1.0	/	0.7	/	1.5	0.1	/	0.4	/	143
6; WI; 10	700	1400	/	/	11.0	4.2	5.6	/	4.0	6.5	2.4	3.0	/	2.2	/	/	/	/	/	144
5-7; WI; 15	700	1500	CH_4/Ar-90/10	Δ: He	9.0	6.0	/	/	/	8.0	5.1	/	/	/	7.0	4.1	/	/	/	41
10-12; WI; 15	700	1550	CH_4/N2-91/9	Two steps: Δ: H_2/CH_4-91.5/8.5. then Δ: He	11.0	6.5	/	/	/	9.4	7.6	/	/	/	9.4	7.6	/	/	/	116
6; IE (ultrasounds); 11.5	700	1500	CH_4/N_2-80/20	Δ: CH_4/N_2-80/20	14.3	4.1	/	/	4.0	12.1	3.7	/	/	4.8	/	/	/	/	/	145
5; superciritcal solvothermal; 11.5	700	1500	CH_4/N_2-80/20	Δ: CH_4/N_2-80/20	15.1	5.6	/	/	/	13.6	5.7	/	/	/	12.4	5.5	/	/	/	146
3; WI; 15	700	1350	CH_4/N_2-90/10	Δ: He	6.7	3.5	/	0.1	1.5	3.8	2.4	/	0.3	0.5	/	/	/	/	/	117
Single-site Mo@HZSM-5 catalyst																				
0.5; Mo-HT; 110	850	2500	CH_4-N_2-80/20	Δ: CH_4/N_2-80/20	3.0	/	0.4	0.9	/	3.7	/	0.2	1.1	/	3.9	/	0.1	0.8	/	147
Mo/TNU-9 catalysts																				
6; MM; 4	700	1387	CH_4/N_2-92.5/7.5	Δ: CH_4/N_2-92/8	14.5	5.7	9.5	/	/	10.5	4.9	7.0	/	/	/	/	/	/	/	148

6; MM; 25	700	1387	CH_4/N_2-92.5/7.5	Δ: CH_4/N_2-92/8	11.0	5.0	6.0	/	4.8	9.1	4.7	5.5	/	3.5	/	/	/	/	/	[149]
Mo/IM-5 catalysts																					
4; WI; 25	700	1387	CH_4/N_2-92.5/7.5	Δ: CH_4/N_2-92/8	11.2	/	6.0	/	/	8.0	/	4.8	/	/	/	/	/	/	/	[150]
4; MM; 25	700	1387	CH_4/N_2-92.5/7.5	/	12.0	/	7.3	/	/	10.5	/	6.3	/	/	8.5	/	5.6	/	/	[151]
Mo/ITQ-2 catalysts																					
3; WI; 25	700	1500	CH_4/N_2-90/10	Δ: He	7.3	2.3	3.0	0.1	4.0	4.0	1.8	2.3	0.2	1.4	/	/	/	/	/	[152]
HZSM-5 (core)-Silicalite-1 (shell, 13.2 wt %) catalysts																					
6; WI; 15	720	1500	CH_4/N_2-90/10	Δ: He	15.0	7.2	12	/	/	12.7	7.7	11.7	/	/	10.6	7.0	10	/	/	[153]
Mo/Sulfated Zirconia catalysts																					
5; WI; /	650	600	CH_4/Ar-67/33	Δ:H_2 then CH_4/H_2-20/80 (4 h) at 650 °C	17.3	2.4	/	1.6	/	14.2	1.7	/	1.5	/	11.0	0.8	/	1.1	/	[154]

[1]If not indicated, it is atmospheric pressure, WI: wet impregnation, MM: mechanical mixing, MF: melting fuse, HT: hydrothermal treatment, IE: ionic exchange; Δ: difference from the room temperature to the reaction temperature; feed composition is presented in vol %/vol %.

So far, based on numerous studies and results summarized in review papers it is accepted that the Mo/HZSM-5 is the most suitable MDA catalyst to upgrade methane into valuable aromatics.[3–22] However, the mechanism of methane dehydroaromatization on the Mo/HZSM-5 catalyst is still under discussion. Two different paths are actually considered: (i) a bifunctional mechanism involving the coupling of methane to C_2H_x species on molybdenum sites, followed by the oligomerization of these intermediates to aromatics on Brønsted acid sites [4,7,155], or (ii) a hydrocarbon pool mechanism involving the activation of methane on molybdenum sites reacting with hydrocarbons entrapped in the zeolite pores responsible for the aromatics formation.[112,156] A typical MDA reaction on the Mo/HZSM-5 catalyst can be divided in three steps[156] including (i) the activation of the catalyst corresponding to molybdenum oxides reduction without benzene production, (ii) the increase of benzene formation during the induction period, and finally (iii) the constant benzene production and progressive deactivation of the catalyst.

One of the main role of the Mo/HZSM-5 catalyst is the shape-selective production of benzene from oligomerization of light hydrocarbons intermediates in the zeolite micropores. A wide range of molybdenum species have been proposed as active sites for the methane activation[11,141,157–165] and they can be summarized in two groups: (1) the partially reduced oxy-carbides species $[MoO_xC_y]^{n+}$ and (2) molybdenum carbides (MoC_x). The state of the metallic active species in terms of location, evolution with time and activity are complex due to their diversity and vast formation of coke during the MDA reaction. So far, a general scheme representing anchoring of mono ($[MoO_2]^{2+}$) and dimeric ($[Mo_2O_5]^{2+}$) molybdenum oxides to BAS, and a deposition on the external surface of the catalysts resulting in the formation of a MoO_3 oxide layer is accepted.[166,167] The mode of anchoring and location of molybdenum is sensitive to the Mo/Al balance, *i.e.*, at low Mo/Al ratio the molybdenum

forms mainly $[MoO_2]^{2+}$ species, while the high Mo/Al favors the formation of dimeric species and deposition of bulk oxides on the external surface of the catalysts.[114,157,166] Molybdenum oxides anchored on Brønsted acid sites are reduced to mono or dimeric oxy-carbides during the activation period under methane flow through a multi-stage reduction while producing mostly H_2 and CO.[156,158,165,167–169] Their deeper reduction into carbides is not required in order to produce benzene.[169,170] The dispersion of molybdenum in the Mo/HZSM-5 is the most critical to have an active and stable catalyst.[141,155,159,171,172] The zeolites with low Si/Al ratio provide more anchoring sites, leading to a homogeneous dispersion of Mo, while a high silicon content or high molybdenum loading resulted in the formation of MoO_x clusters and weak linkage with the framework oxygen.[110,157,172,173] The weak interaction between molybdenum and the support lead to molybdenum migration and aggregation during the pretreatment of the catalysts (high temperature treatment) or during the MDA reaction.[109,174] In order to prepare well-dispersed metal containing catalysts by impregnation, the balance between the molybdenum and the Si/Al ratio of the zeolite (*i.e.* Mo/Al molar ratio) must be considered carefully.

Recent reviews emphasized on two disadvantages restricting the industrial development of the non-oxidative transformation of methane.[8,12,18] First, the MDA reaction is thermodynamically limited with a maximum of benzene conversion of 12.5% at 700 °C, thus the Mo/HZSM-5 catalysts show low activity. Second, the coke formation at the high temperatures of the reaction is favored, leading to the fast deactivation of the catalyst and limiting the benzene selectivity. Thus, some aspects of the MDA process with emphasis on catalyst engineering (dopant, post-synthesis treatment), pretreatment, regeneration and co-feed of oxidative or reducing species have been considered. These features will be critically analyzed in the following sections in terms of deactivation and improvement of benzene formation in the MDA reaction.

3.2. Deactivation of MDA catalyst and mitigation strategies

3.2.1. Modes of MDA catalysts deactivation

Despite the substantial research efforts on MDA catalysts development, the deactivation remains a significant concern. Two ways of deactivation lead to the significant loss of catalysts performance: (i) the reversible coke formation during the MDA reaction and (ii) the irreversible structural damage including the formation of $Al_2(MoO_4)_3$ and carbide migration due to the harsh experimental conditions of the MDA process. Therefore, during the past decade, a variety of approaches have been developed to extend the catalyst lifetime.

3.2.1.1. Reversible coke formation in MDA catalysts

The Mo/HZSM-5 catalysts suffer from solid carbon formation during the MDA reaction, at selectivity reaching from 10 to 50%.[108,110,113,117,137,144,145] The characterization and quantification of the coke are crucial to understand the deactivation mechanism of the catalysts. The most common TGA/DTA characterization technique provides an important information about the coke formed on the catalysts allowing to discriminate three kinds of carbonaceous deposits: (i) the carbon in molybdenum carbides, burning between 400 and 450 °C (not considered as a coke), (ii) the carbon associated to a "soft" coke, burning around 450 - 500 °C, and (iii) the carbon related to a "hard" coke burning between 500 and 600 °C.[8,12,44,160] The thermal analysis only provided quantification and usually are coupled with complementary TEM[118], Raman[172,175] or XPS[175] spectroscopy characterization methods in order further to investigate the localization and nature of the carbonaceous deposit. Most of the studies considered "soft" and "hard" cokes separately, whose discrimination comes from the extrapolation of their oxidation temperatures measured by the thermal analysis. Both cokes have an aromatic nature[156,168], but have different locations in the zeolites thus impacting the combustion temperature. However the exact location, nature and the effect of coke on the MDA catalysts remain ambiguous.

Due to its lower combustion temperature, the “soft” coke is supposed to be located either (i) on the external surface of the zeolite crystals where oxygen access is not limited by diffusion, and/or (ii) close to the molybdenum sites, able to catalyze the coke combustion.[41,54,160,168,172,176] The soft coke was reported to have a graphitic like carbon structure.[41,160,172] The growth of graphitic like carbon close to the molybdenum carbide particles is causing deactivation of the MDA catalyst. Molybdenum carbides are the actives species involved in the methane activation and as time on stream increases, coke coverage lead to a loss of the catalysts activity.[160,177] Furthermore, molybdenum carbides migrated from pore mouths to the external surface of zeolite crystals and sinter after a long time on stream, enhanced by the “soft” coke formation.[118,178] Molybdenum carbides and Brønsted acid sites at the external surface of the catalysts promoted the growth of the “soft” coke.[44,111,118,159,172,178–180] As depicted in **Figure 5**, the amount of graphitic coke on the catalyst is independent to the molybdenum - Si/Al balance of the catalysts. If an increase of the external molybdenum carbide particles with higher molybdenum content is considerd, resulting from the synthesis or migration during the MDA reaction [166], the formation of soft coke on molybdenum carbides will be minor. The graphitic carbon formation must occur through the thermocatalytic scission of methane on the external surface[156,175,181], moreover to be catalyzed by the solid carbon deposit himself.[182]

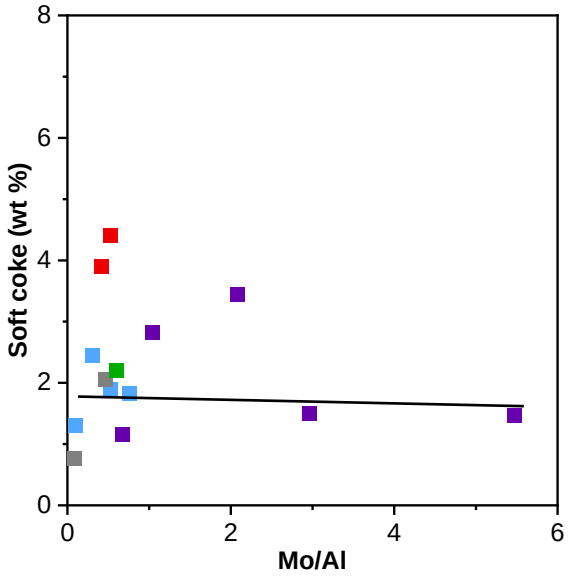

Figure 5. Content of soft coke in Mo/HZSM-5 as a function of the Mo/Al molar ratio of catalysts after the MDA reaction. Results are adapted for blue: from Ref[41], grey: from Ref[168], red: from Ref[183], green: from Ref[111] and violet: from Ref[172].

The passive thin layer growth of coke at the external surface blocks the zeolite micropores and mitigates the access of the BAS to the intermediates and reactants.[118,172,176] Additionally, it was demonstrated that the production of the "soft" coke is proportional to the external surface of the mesoporous catalysts obtained by desilication or swelling of MFI type zeolite crystals (**Figure 6**).

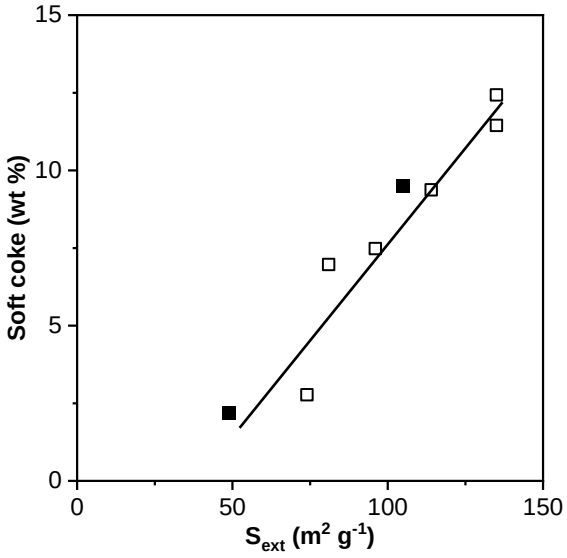

Figure 6. Content of soft coke in desilicated[111] (■) and lamellar[184] (□)Mo/HZSM-5 catalysts as a function of their external surface area after the MDA reaction.

"Soft" coke is not only a deactivating deposit but active in the ethylene transformation towards production of aromatics.[167]

"Hard" coke was reported to have a polyaromatic structure and is supposed to grow in the micropores through acidic catalysis and burn at higher temperatures due to a low oxygen accessibility.[12,41,54,160,168,175,181] The polyaromatic coke accounts for most of the total coke weight deposited on the catalyst.[11,168,175,181,185] It should be noted that thermal quantification of "hard" coke gives an underestimated value of polyaromatic coke as these species are also formed on the external surface and account for the "soft" coke.[118,186] Polyaromatic coke formation occured through benzene and ethylene polycondensation on the Brønsted acid sites in the micropores of zeolites.[53,175,181,187–189] Thus, a higher amount of free Brønsted acid sites (*i.e.* low Mo/Al molar ratio) in the zeolite catalysts promotes the formation of "hard" coke (**Figure 7**). The "hard" coke amount increases with time on stream and gradually fill the zeolite porous network, resulting in a zeolite templated carbon (ZTC) like structure and full pore clugging.[168] Polyaromatic coke formation lead to activity loss through diffusion of molecules in the micropores and coverage of the Brønsted acid sites.[10,172] The negative impact of the "hard" coke on the MDA reaction is regarded as entrapped polyaromatic species formed in the induction period and play a role in the benzene formation.[156,168]

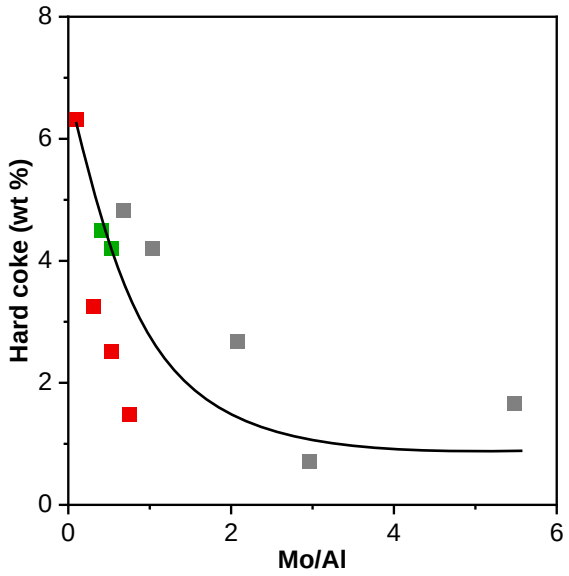

Figure 7. Content of hard coke in Mo/HZSM-5 as a function of the Mo/Al molar ratio of catalysts after the MDA reaction. Results are adapted for grey: from Ref[172], red: from Ref[41] and green: from Ref[183].

The properties of coke(s) in terms of way of formation, location, nature and impact on MDA are still a matter of discussion.[8,168] This raises the question of cokes nomination, *i.e.* from the semantic point of view, the names "hard" and "soft" cokes can mislead and suggest that one is more detrimental for MDA than the other. Nevertheless, these names come from the differences in combustion temperatures observed during the TG analysis, and their respective toxicities are not established yet. Most of the studies considered the zeolite network obstruction point of view and a few studies report on rational and rigorous correlations between coking and activity loss of catalysts. This is mainly due to the complexity of characterizing of used Mo/HZSM-5 catalysts by *operando* spectroscopic methods for MDA[6] and TG/DTA analysis. The temperature of coke combustion depends on several parameters like the zeolite acidity, crystal size, coke content, metal content and time on stream.[110,168,172,181,190] Further investigations on space and time evolution of carbonaceous species during the MDA process are highly desirable by combination of characterization techniques.[6] Kinetics studies of coke formation (carbonaceous deposits) in the catalyst

followed by ex-situ analysis will provide important information.[191–193] Such studies will provide information on reactive intermediates while clarifying the ambiguous discrimination between coke and hydrocarbon pool. New approaches are needed, such as addressing the deactivation problem from a coke toxicity point of view[167], *i.e.* active sites poisoning and not only focusing on the pore blocking issues.

In summary, coke formation during the MDA reaction is one of the main feature hindering the process development and is a major concern of hydrocarbons processing, especially on acidic catalysts. The development of a regeneration step to remove the coke from the catalyst is a very important issue toward MDA process optimization.[194] The nature and formation rate of coke is related to the properties of the catalyst and operating conditions. Numerous solutions have been considered to mitigate the coke formation and deactivation rate during the past decades but still the exact role and mechanism of formation of polyaromatic hydrocarbons require further investigations in order to develop an efficient MDA process.

3.2.1.2. Irreversible structural damages of MDA catalysts

The excessive heat treatment and the presence of water during the severe MDA reaction and especially during the regeneration step lead to irreversible deteriorations of the catalyst; the classical example is the Mo/HZSM-5. Under thermal and oxidizing conditions, the Mo species became mobile and can migrate on the external zeolite surface to form molybdenum clusters or react with the framework Al to produce aluminium molybdates ($Al_2(MoO_4)_3$), thus leading to pores blocking.[114,140] External molybdenum species ($Al_2(MoO_4)_3$ and MoC_2) are considered as spectator in the MDA reaction, resulting in irreversible deactivation of the catalyst.[166,167] Furthermore, the molybdenum sintering caused a decrease of methane conversion rate[118] as the density of active sites decreased, and the synergetic effect of Mo-BAS proximity is lost.[109] Then the Mo migration prevents continuous regeneration and

recycling of the catalyst, which is crucial due to the rapid formation of coke. The robustness of impregnated Mo/HZSM-5 catalyst is inherent in the zeolite framework in the presence of alumina. To mitigate the irreversible deactivation of the catalyst, the Mo-support interactions, *i.e.* the balance between Mo and Si/Al ratio of the zeolite is a critical parameter to be considered.[116,140,166,195] High molybdenum content favors migration phenomena, and the optimal molybdenum content for the HZSM-5 catalyst with a Si/Al ratio of 15 was found to be around 4 - 5 wt %.[41,109,166,174] Thus, better molybdenum anchoring to the zeolite framework obtained with low Si/Al ratios offsets the weaker (hydro)thermal stability of aluminum-rich zeolites.[196,197] As an alternative way, the preparation of atomically dispersed Mo/HZSM-5 catalysts by defects "healing" of the framework structure with molybdenum was reported.[147,198–200] The Mo was introduced in the silanol nest defects of the MFI zeolite framework resulting in ultra-stable catalysts. The atomically dispersed Mo/HZSM-5 depicted high stability of both the zeolite structure and molybdenum during multiple cycles of MDA reaction at 850 °C and regeneration at 750 °C under steaming. Several other strategies have been proposed to improve the stability of the catalyst during regeneration and to adapt molybdenum-containing zeolites to harsh regeneration conditions.[8]

3.2.2. Evolution of the catalyst stability during the MDA

3.2.2.1. Impact of the catalyst pretreatment

The route of formation of molybdenum active sites is a crucial parameter in designing a stable and active Mo/HZSM-5 catalyst. The carburation of molybdenum at temperatures below that of the MDA reaction (< 650 °C) appeared to be beneficial for the catalytic performance as the reduced forms are less volatile than the oxidized forms.[201] Thus, heating the fresh catalyst, *i.e.* with molybdenum in oxidized form, above 550 °C under inert (N_2, He) or oxidative (O_2) atmosphere may lead to materials damage through molybdenum sintering

and migration at the external surface. Moreover, mobile molybdenum species can extract aluminum from the zeolite framework and form extra-framework $Al_2(MoO_4)_3$ species.[45,111,140] Molybdenum carbides clusters resulting from external molybdenum oxides reduction and $Al_2(MoO_4)_3$ species are considered as spectators for the MDA cause coke formation.[114,166,167,202] On the other hand, the heating of the Mo/HZSM-5 catalyst under a reductive atmosphere such as pure flow of CH_4, H_2, CO or a CH_4/H_2 mixture shown improvement of the catalyst stability and an increase of the benzene yield.[43–46,49,183,203] In these conditions, the reduction of Mo sites occurred at lower temperatures, preventing the Mo migration.[43] Recently, Rahman *et al.*[43] reported the effect of different pretreatment atmospheres including He, CH_4, H_2 and a mixture of CH_4/H_2 on the structural properties and performance of MDA catalysts. Higher Mo dispersions were correlated with lower reduction temperatures. Pretreatments under a mixture of CH_4/H_2 (10/90, v/v) or pure H_2 followed by carburization under CH_4 at 700 °C led to the best performance of the catalyst. Furthermore, with H_2 in the flow, no coke formation was observed during the carburization process, while with pure CH_4 flow, soft coke was produced close to molybdenum active sites.[118]

3.2.2.2. Impact of the reaction conditions

In addition to the catalyst' properties, the operating conditions impact the coke formation and the catalyst deactivation behavior. Rates of coke formation and catalyst deactivation are faster at high space velocity[188,204], *i.e.* low contact time, thus suggesting that coke formation is not kinetically limited. However, the amount of coke is lower at high space velocities and shifts towards external surface coverage, facilitating the removal by lower temperature oxidation.[188,204] Moreover, high space velocity induces mass transfer limitations over the zeolite crystals, thus the coverage of their surface enhances the deactivation.[188,204]

Thermodynamically, the formation of polyaromatics and carbon graphite is more favorable than benzene at higher temperatures.[8,205] Experimentally, raising the reaction temperature by 60 °C multiplied by three-fold the total coke amount generated on the spent catalyst.[206]

The general chemical equation for polyaromatics compounds formation is as follow:

$$x\mathrm{CH_4} \rightleftarrows \mathrm{C}_x\mathrm{H}_{x-2(\mathrm{n}-1)} + \left(\frac{3}{2}x + \mathrm{n} - 1\right)\mathrm{H_2} \qquad \textbf{(2)}$$

were n is the number of aromatic cycles in the final molecule.

It can be seen from equation (2), increasing the pressure will shift the thermodynamic equilibrium to indirect way according to the principle of Le Chatelier. The longer is the polyaromatic coke molecule, the more significant will be the effect of pressure on polyaromatics growth. However, the scavenger effect of hydrogen shade off with equilibrium shifting, which can indirectly increase coke accumulation on Brønsted acid sites.[207] Hensen *et al*. [208] showed that the selectivity shifted towards benzene formation, and the mitigation of coke formation and deactivation of the catalyst with increasing the pressure. Surprisingly, the coke content recovered on the spent catalyst after 900 min of reaction was higher at elevated pressure. It has been proposed that higher pressures favors coke formation in the zeolite pores with more dense carbon structures formed, thus, the combustion temperatures shifted to higher values.

3.2.2.3. Impact of the regeneration steps

The coke formation cannot be entirely avoided due to the acidic nature of the catalyst and the reactivity of unsaturated products formed under the high temperature MDA reaction. The total coke removal can be reached at high temperatures treatment up to 600 °C as shown by TG analysis. The oxidation of coke involved as well the oxidation of molybdenum carbides to molybdenum oxides occurring around 400 - 450 °C. Above 500 °C, the molybdenum oxides became volatile and started to migrate, leading to materials damages through MoO_x

sintering or formation of extra-framework $Al_2(MoO_4)_3$ species[45,111,140] that depend on the molybdenum content in the catalysts.[157,209]

Different strategies for regeneration of MDA catalyst have been evaluated in order to remove efficiently the coke while minimizing the damage of the catalyst' structure. One strategy is based on burning the coke at lower temperatures. Using 2 vol % of NO as a promoter in air, the total removal of coke at a lower temperature, *i.e.* 450 °C instead of 550 °C was achieved and this allowed to mitigate the loss of activity during eight reaction-regeneration cycles in comparison with the catalyst simply treated in air only.[42] However, the study of the regeneration temperature on the performance of MDA catalyst revealed that the total coke removal was not needed to recover the initial activity.[41] The catalyst treatment at 450 °C under 10 vol % O_2 in He removed the "soft" coke and allowed to recover similar methane conversion and benzene yield after 5 cycles of 10 hours reaction followed by regeneration. This implies that the "soft" coke is highly toxic for the catalyst. On the contrary, at higher temperatures (550, 700, and 850 °C), the coke removal was more efficient but involved irreversible structural damages like a loss of molybdenum and Brønsted acidity leading to a decrease of benzene production in multi-cycle catalytic reaction.

In comparison, the coke removal under a reductive atmosphere was shown to occur at higher temperatures (700-800 °C) but re-carburization of the catalyst was not needed.[41,209–211] Regeneration under H_2 partially removed the coke by methanation while allowing to recover part of the benzene yield and methane conversion. Contrarily to oxidative treatment, the H_2 coke-removal did not cause irreversible damage to the catalyst.[209] Indeed, molybdenum was preserved at a reduced state and no water was formed, while in the case of oxidative treatment, water from the coke combustion caused dealumination.[140,212] Despite these considerations, a reductive treatment was found to be less effective than the low-temperature

oxidative treatment in terms of catalyst' deactivation after several MDA/regeneration cycles.[41]

Another way towards improvement of MDA catalysts reported is to conduct the process under "short" cycling conditions by starting the regeneration of the catalyst before reaching the total deactivation. Alternative 1.5 h of reaction then 0.5 h of regeneration at 540 °C led to a maximum benzene yield with productivity three-fold higher than in a single run over 18 h experiment.[144] However, the carburization was required to prevent molybdenum oxides migration after the regeneration in these conditions. Furthermore, as observed during experiments with high-frequency injection of dioxygen in the MDA feed, the frequency of the cycles was the parameter that must be carefully optimized.[213]

3.3. Improving aromatic production in the MDA

3.3.1. Addition of promoters

The introduction of several metals as promotors to tune the performance of the Mo/HZSM-5 catalysts was studied. The concentration of the promoters was varied, and either single or bimetallic promoters were used. The total benzene yield reported on bi-metallic Mo-X/HZSM-5 catalysts and the first order deactivation rate constant of benzene formation are summarized in **Table 3**. The bi-metallic Mo-X/HZSM-5 based catalysts contain palladium, ruthenium, iridium, zinc, copper, chromium, tungsten, platinum, iron, cobalt, nickel, rhenium or gallium (**Table 3**). In most of the studies, mono- and bi- metallic catalysts with an increase of the total metallic content were compared. To account the effect of the promotor (metal content), the increase of benzene formation per moles of metal in comparison with the monometallic molybdenum catalyst (Mo/HZSM-5) used as a reference was calculated according to the following equation 3:

$$\tau_{\text{Benzene}} = \frac{\left(\frac{\text{Yield}_{\text{Benzene}}}{\text{n}_{\text{metal}}}\right)_{\text{Bimetallic}}}{\left(\frac{\text{Yield}_{\text{Benzene}}}{\text{n}_{\text{metal}}}\right)_{\text{Monometallic}}} \quad \textbf{(3)}$$

The results are depicted in **Figure 8**.

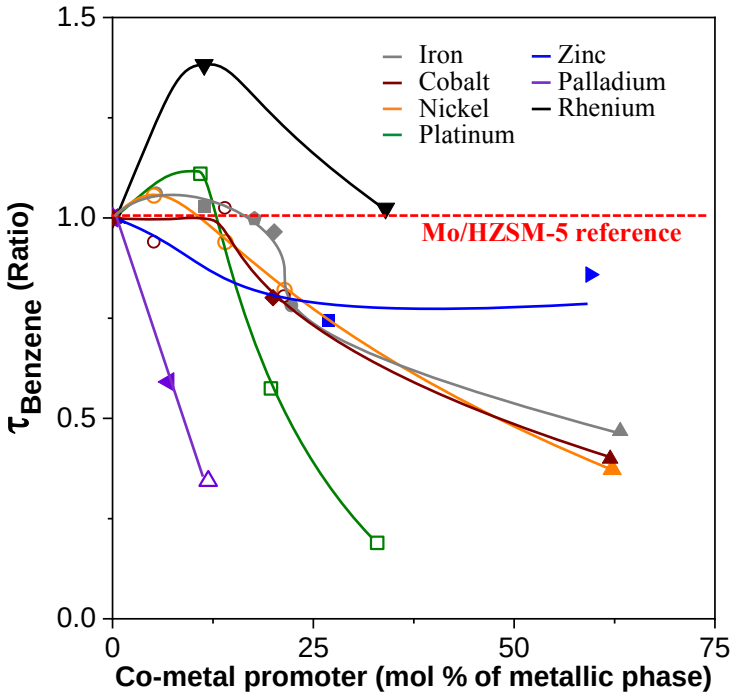

Figure 8. Effect of the concentration of co-metal promotors (Fe, Co, Ni, Pt, Zn, Pd and Rh) of Mo/HZSM-5 catalysts in comparison with the monometallic molybdenum catalyst (Mo/HZSM-5 reference, dashed red line) on benzene yield.

Table 3. Performances of Mo/HZSM-5 catalysts doped by metals promoters in MDA reaction.

Co-metal	**Composition**	**Si/Al**	**Co-metal in the metallic phase**	**MDA conditions**		**TOS. range**	$\mathbf{Y_{C_6H_6}}$	**Increase of benzene yield relative to Mo/HZSM-5 ($\tau_{Benzene}$)**	$\mathbf{k_d^{C_6H_6}}$	**Symbol/ References**
				T	**Feeding conditions**					
	wt %		Mol %	°C		h	%		h^{-1}	
/	**2Mo**		**0.0**				**0.5**	**1.0**	**$8.3\ 10^{-2}$**	
Pd	2Mo-0.3Pd	14	11.9	700	WHSV: 2700 h^{-1}	0.2-24.1	0.2	0.3	$6.7\ 10^{-2}$	Δ/[214]
Ru	2Mo-0.3Ru		12.5				0.9	1.7	$7.2\ 10^{-2}$	
/	**6Mo**		**0.0**				**3.6**	**1.0**	**$1.1\ 10^{-1}$**	
Pd	6Mo-0.5Pd		7.0	700	GHSV: 1500 ml g_{cat}^{-1} h^{-1}	0.1-4.0	2.3	0.6	$4.7\ 10^{-1}$	◀/[215]
Ir	6Mo-0.5Ir		4.7				1.3	0.3	$2.4\ 10^{-1}$	
/	**6Mo**	25	**0**	700	GHSV: 1500	0.1-	**3.2**	**1.0**	**$9.5\ 10^{-1}$**	▶/[137]

Zn	3Mo-3Zn		59.5		ml g_{cat}^{-1} h^{-1}	4.0	3.4	0.9	$1.1\ 10^{-1}$	
Cu	3Mo-3Cu		60.2				1.9	0.5	$9.5\ 10^{-2}$	
/	**6Mo**		**0.0**				**4.0**	**1.0**	**$3.0\ 10^{-2}$**	
Cr	3Mo-3Cr	**25**	64.9	700	GHSV: 1500 ml g_{cat}^{-1} h^{-1}	0.4-4.0	4.4	0.8	$3.4\ 10^{-2}$	/[216]
W	3Mo-3W		34.3				3.4	1.1	$1.8\ 10^{-1}$	
/	**2Mo**		**0.0**		GHSV: 1620 ml g_{cat}^{-1} h^{-1}		**4.9**	**1.0**	**$1.6\ 10^{-1}$**	
Pt	2Mo-0.5Pt	35	10.9	700	CH_4/Ar-90/10 vol %/vol %	0.1-6.1	6.2	1.1	$4.0\ 10^{-1}$	□/[47]
	2Mo-1Pt		19.7				3.5	0.6	$1.7\ 10^{-1}$	
	2Mo-2Pt		33.0				1.4	0.2	$1.7\ 10^{-1}$	
/	**6Mo**		**0.0**		GHSV: 1500 ml g_{cat}^{-1} h^{-1}		**5.7**	**1.0**	**$1.8\ 10^{-2}$**	
Fe	6Mo-0.2Fe	15	5.4	700	CH_4/N_2-91/9 vol %/vol %	0.5-10.2	6.4	1.1	$7.0\ 10^{-4}$	●/[49]
	6Mo-1Fe		22.3				5.8	0.8	$2.9\ 10^{-3}$	
/	**6Mo**		**0.0**				**5.6**	**1.0**	**$1.9\ 10^{-2}$**	
Co	6Mo-0.2Co		5.1				5.5	0.9	$1.3\ 10^{-2}$	
	6Mo-0.6Co		14.0		GHSV: 1500 ml g_{cat}^{-1} h^{-1}		6.7	1.0	$4.0\ 10^{-4}$	
	6Mo-1Co	15	21.3	700	CH_4/N_2-91/9 vol %/vol %	0.1-9.9	5.7	0.8	$1.1\ 10^{-3}$	○/[45]
Ni	6Mo-0.2Ni		5.2				6.2	1.1	$9.6\ 10^{-3}$	
	6Mo-0.6Ni		14.1				6.1	0.9	$3.2\ 10^{-3}$	
	6Mo-1Ni		21.4				5.8	0.8	$4.5\ 10^{-3}$	
/	**8Mo**		**0.0**		GHSV: 1440 ml g_{cat}^{-1} h^{-1}		**5.9**	**1.0**	**$6.6\ 10^{-1}$**	
Fe	8Mo-1Fe	25	11.1	800	CH_4/CO_2/Ar-90/2/8 vol %/vol %/vol %	0.3-1.0	7.2	1.0	$3.0\ 10^{-1}$	⬟/[217]
/	**6Mo**		**0.0**				**3.6**	**1.0**	**$1.5\ 10^{-1}$**	
Co	3Mo-3Co	25	61.9	700	GHSV: 1500 ml g_{cat}^{-1} h^{-1}	0.1-4.0	1.9	0.4	$3.2\ 10^{-1}$	▲/[139]
Ni	3Mo-3Ni		62.2				1.8	0.4	$3.3\ 10^{-1}$	
Fe	3Mo-3Fe		63.2				2.3	0.5	$2.6\ 10^{-1}$	
/	**4Mo**		**0.0**		GHSV: 3000 ml g_{cat}^{-1} h^{-1}		**1.6**	**1.0**	**$9.5\ 10^{-2}$**	
Re	4Mo-1Re	23	11.4	700	CH_4/N_2-85/15 vol %/vol %	0-13.2	2.5	1.4	$8.0\ 10^{-2}$	▼/[135]
	4Mo-4Re		34.0				2.5	1.0	$6.6\ 10^{-2}$	
/	**4Mo**		**0.0**		GHSV: 3000 ml g_{cat}^{-1} h^{-1}		**3.4**	**1.0**	**$4.8\ 10^{-2}$**	
Zn	4Mo-1Zn	27.5	26.8	700	CH_4/Ar-90/10 vol %/vol %	0.3-11.7	3.5	0.7	$4.9\ 10^{-2}$	■/[48]
Fe	4Mo-0.3Fe		11.4				4.0	1.0	$2.2\ 10^{-2}$	
/	**3Mo**		**0.0**		GHSV: 1200 ml g_{cat}^{-1} h^{-1}		**1.7**	**1.0**	**$1.1\ 10^{-1}$**	
Co	3Mo-0.46Co	40	20.0	700	CH_4/N_2-80/20	0.2-5.7	1.7	0.8	$4.3\ 10^{-2}$	◆/[218]
Fe	3Mo-0.44Fe		20.1				2.0	1.0	$4.2\ 10^{-2}$	

Ga	3Mo-0.54Ga	19.8	vol %/vol %	2.0	0.9	$1.1\ 10^{-1}$	

Bold: monometallic catalysts used as references for the catalyst series; [1]benzene produced (%) is calculated by integration of a range of T.O.S specified for each case.

The general trend observed is that adding a small amount of co-metal promotors to the Mo/HZSM-5 catalyst is beneficial (**Figure 8**). Below 20 mol % of co-metals in the metallic phase, the deactivation rate of benzene formation is decreased, except in the cases when palladium and iridium were used (**Table 3**). However, the benzene production per moles of metals is only slightly improved in the presence of platinum, rhenium, nickel or iron added to the Mo/HZSM-5 catalyst at content below 20 mol %.

3.3.2. Addition of co-feed reactant

The addition of a co-reactant to the MDA feed to extend the catalyst lifetime by mitigating the coke formation has been investigated. In most studies, H_2, CO, CO_2 and H_2O as co-feed reactants were employed.

To evaluate the impact of a co-feed reactant, the increase of benzene formation in comparison with the absence of a co-feed was calculated according to the equation 4:

$$\tau_{\text{Benzene}} = \frac{(\text{Yield}_{\text{Benzene}})_{\text{With co-feed reactant}}}{(\text{Yield}_{\text{Benzene}})_{\text{Without co-feed reactant}}} \quad \textbf{(4)}$$

The impact of a co-feed reactant on the "relative conversion" of methane ($X_{CH_4}^{Rel}$) according to the thermodynamic equilibrium at the reaction temperature was calculated according to the equation 5:

$$X_{CH_4}^{Rel} = \frac{(X_{CH_4})_{\text{With co-feed reactant}}}{(X_{CH_4})_{\text{Thermodynamic equilibrium}}} \quad \textbf{(5)}$$

3.3.2.1. Addition of H_2 co-feed reactant

The addition of H_2 in MDA feed has been studied over a wide range of concentrations, from 0.5 to 30 vol %. The improvement of Mo/HZSM-5 catalysts in terms of methane conversion and benzene formation rate with different flow composition of H_2 is depicted in

Figure 9. The addition of H_2 has a positive effect on catalyst' stability at lower than 3 vol % H_2 in the feed (**Figure 9**). Moreover, the amount of coke on the catalysts decreased with the addition of H_2 in the feed, and most notably, the polyaromatic coke located in the zeolite channels decreased.[175,188,219–221] As discussed in the previous section, the H_2 co-feed shifts the equilibrium of the methane pyrolysis reaction towards reactants according to Le Chatelier principle and limits the formation of the "hard" coke. Moreover, the hydrogen favors the desorption of aromatic species from BAS, which mitigates coke formation during toluene disproportionation for exemple.[222,223] Above 3 vol % H_2, the initial conversion and benzene formation rate are negatively affected as shown in **Figure 9**. The addition of H_2 in the feed shifts the equilibrium of MDA reaction according to the equation 1. Thus, the higher the H_2/CH_4 ratio is, the lower the CH_4 conversion is expected[219]; the performance of the catalyst decreases linearly with the H_2/CH_4 ratio (**Figure 9**). As shown by equation 2, the coke formation is more affected by hydrogen co-feed than the benzene formation, *i.e.* the hydrogen (moles) produced per aromatic ring is higher in the case of coke than for benzene. Therefore, H_2 co-feed is only efficient at low content (< 3 vol %) where the MDA reaction is not affected substantially and the formation of polyaromatic coke is mitigated.

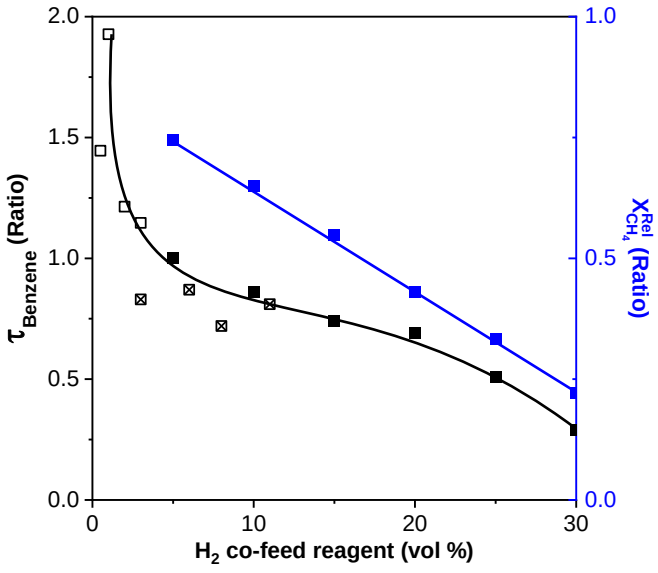

Figure 9. Impact of the amount of H_2 co-feed reactant in Mo/HZSM-5 catalysts on the benzene formation (black symbols) and "relative conversion" of methane (blue symbols). Data taken for ■: from Ref[175], □: from Ref[50] and ⊠: from Ref[51].

3.3.2.2. Addition of CO co-feed reactant

The effect of carbon monoxide addition over a range of 1- 12 vol % in the feed to the MDA reaction has been studied extensivly.[52,53,115,224–227] The impact of the CO co-feed reactant on the initial methane conversion and benzene formation rate is presented in **Figure 10**. An enhancement of the catalysts performance under addition of CO with concentrations from 1 to 12 vol % was observed, which is consistent with the lower amount of coke deposited on the catalyst with higher CO concentrations in the feed.[53,115,224]

CO acts as a promoter in MDA reaction due to different reasons.[52,225] The dissociative adsorption of CO on metallic sites lead to (i) inhibition of the deactivation of molybdenum active sites by oxidation of coke precursors to CO and CO_2 and (ii) formation of hydrocarbon products from the reaction between adsorbed carbon atoms and dihydrogen produced during the MDA.[115,225] Thus, hydrogen consumption shifts the thermodynamic equilibrium of the MDA reaction according to the equation 1 towards the products formation. The oxygen prevents the coke formation by oxidizing the coke precursors, while regenerating the carbon monoxide. Therefore, by taking into account all previous considerations, the incorporation of a promoter that favors both CO dissociation and avoid the methane thermocatalytic scission could significantly enhance the catalyst stability. Metals used in Fisher Tropsch synthesis[228] such as Iron or Cobalt were reported to be good promoters enhancing catalyst' stability under CO co-feeding.[52,53]

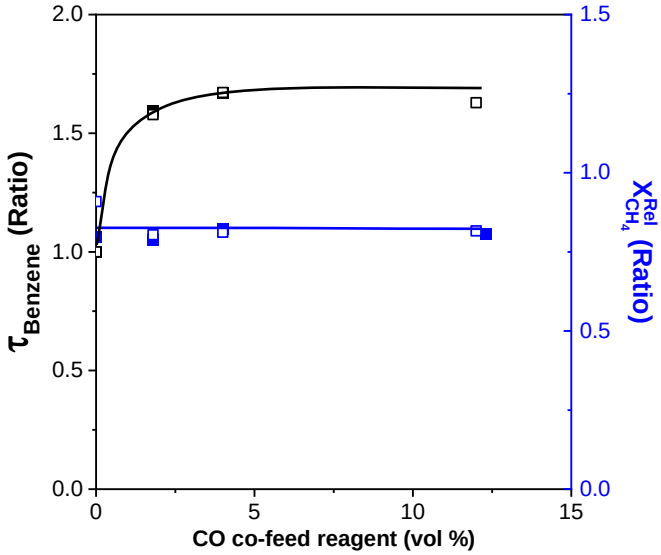

Figure 10. Impact of the amount of CO co-feed reactant in Mo/HZSM-5 catalysts on the benzene formation (black symbols) and "relative conversion" of methane (blue symbols). Data taken for ■: from Ref[52] and □: from Ref[53].

3.3.2.3. Addition of CO_2 co-feed reactant

The use of CO_2 as a co-feed reactant in the MDA is of great importance since it is already present in the natural gas feedstock.[229] The cost of the MDA process could be lowered by eliminating the upstream separation. Moreover, the use of CO_2 as a co-reactant helped to reduce the carbon footprint of the process.[230] The impact of the addition of CO_2 with a concentration in the range 1.6 -14.3 vol % on benzene formation rate and initial methane conversion is presented in **Figure 11**. An improvement of both parameters is observed at CO_2 concentrations lower than 2 vol % in the feed (**Figure 11**), which is mainly due to the presence of H_2 and CO alongside the catalytic bed. Indeed, the addition of CO_2 to the MDA reactor leaded to a staged catalytic bed with (i) upstream dry reforming of methane to produce carbon monoxide and hydrogen or Boudouard reaction with the carbonaceous deposit forming two moles of carbon monoxide and (ii) downstream MDA reaction in the presence of CO and H_2.[53,201,219,224,231,232] Co-feeding with more than 2 vol % CO_2 is detrimental

for the catalytic performance, mainly because of the reoxidation of the molybdenum carbides into oxides by carbon dioxide leading to a decreased of activity.[53,201,219]

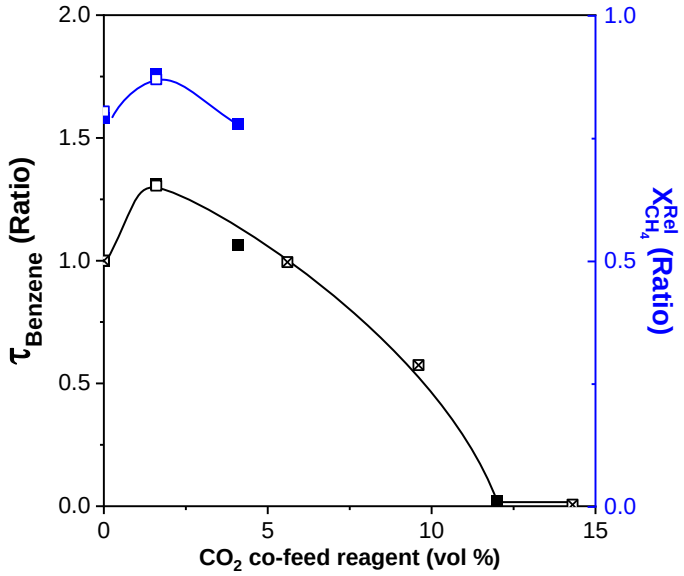

Figure 11. Impact of the amount of CO_2 co-feed reactant in Mo/HZSM-5 catalysts on the benzene formation (black symbols) and "relative conversion" of methane (blue symbols). Data taken ■: from Ref[53], □: from Ref[52] and ⊠: from Ref[233].

3.3.2.4. Addition of H_2O co-feed reactant

The impact of H_2O co-feed reactant on the MDA reaction has been studied at atmospheric pressure with 0.8 - 10.7 vol % H_2O, and a reactor pressure of 3 MPa with 0.6 - 2.6 vol % H_2O in the feed. The effect of the addition of H_2O co-feed reactant on the initial methane conversion and benzene formation rate is presented in **Figure 12**. Water co-feed at low concentration resulted in an improved MDA performance with an optimal value of around 2 vol % in the feed (**Figure 12**). The benefit of using water in the feed is similar to that observed for the CO_2 co-feed reactant. Methane and coke are steam reformed, consuming mainly the coke on the external surface.[54,234] Carbon monoxide and hydrogen are thus produced and act as promoters (see the above sections). However, like CO_2, a high water content in the feed leaded to the reoxidation of the molybdenum carbides. In addition, water favored the dealumination of the zeolite catalysts thus resulting in crystallinity loss.[234,235]

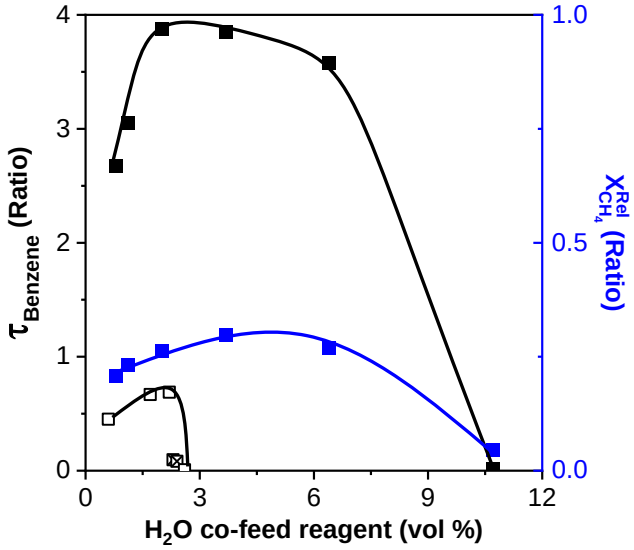

Figure 12. Impact of the amount of H_2O co-feed reactant in Mo/HZSM-5 catalysts on the benzene production (black symbols) and "relative conversion" of methane (blue symbols) Data adapted for ■: from Ref[54], □: from Ref[234] and ⊠ : from Ref[235].

In conclusion, the addition of H_2, H_2O, CO and CO_2 co-feed reactants is an approach to enhance the performance of the catalysts in the MDA reaction. The impact of co-feed reactants on the MDA reaction is summarized in **Table 4**. Importantly, the H_2, H_2O, CO and CO_2 co-feed reactants improved the stability of the catalysts by mitigating the coke formation process. The efficiency of the co-feed reactants on the performance of the catalysts is strongly related to the nature and concentration of the co-reactants.

Table 4. Impact of CO, H_2, CO_2 and H_2O co-feed reactants on the MDA reaction.

Co-feed reactant	Co-feed reactant concentration in the MDA	Positive Impact	Negative Impact	References
H_2	≤ 3	Scavenging of carbonaceous deposits.	/	[175,188,219–221]
	> 3	Equilibrium shift of the reaction from polyaromatic formation towards reactants.	Equilibrium shift of the MDA reaction towards reactants.	
CO	≤ 12[a]	Oxidation of carbonaceous deposit leading to decrease of coke formation. Effect on hydrocarbon products formation.	/	[53,115,224–226]
CO_2	≤ 2	Decoking through Boudouard reaction.	/	[53,201,219,224,231,232]
	> 2	Similar effect observed as for addition of H_2 and CO co-feed reactants.	Deactivation of the molybdenum active sites due to the oxidation of molybdenum carbides into oxides.	
H_2O	≤ 2	Decoking through steam-reforming reaction.	/	[54,234,235]
	> 2	Similar effect observed as for addition of H_2 and CO co-feed reactants.	Deactivation of the molybdenum active sites due to the oxidation of molybdenum carbides into oxides.	

[a]Maximum content reported in the literature.

4. Outlook

Methane is a crucial actor in the energy transition from fossil to renewable resources, initiated in the petrochemical and energetical sectors. This C1 compound is an important building block for the production of higher hydrocarbons. The high hydrogen to carbon ratio in methane allows the production of dihydrogen with low carbon emission. However, the C- H bond strength in methane is much higher than in heavier alkanes or even the C--C bonds, which makes its activation difficult[236]. The C1 chemistry differ substantially from others hydrocarbons, thus requiring the development of new processes. The development of various ways of methane transformation is, therefore, a significant concern, which captivates the scientific community for decades.

Different catalytic ways are actually considered to valorize methane into hydrocarbons and hydrogen, with variable maturity levels. Methane transformation through syngas route is currently operated in different industrial plants. This route involves several steps of transformation to reach the final products, but the different gas-to-liquid technologies offer access for C1 chemistry to a wide range of products: oxygenates, saturated and unsaturated linear hydrocarbons and aromatic compounds. The syngas route has thus a low carbon efficiency and high energy cost. On the contrary, OCM and MDA routes are more elegant and alternatives, as they allow direct and selective production of C2 and benzene, respectively, two essential building blocks of industrial chemistry.

The OCM technology is more mature than MDA, but efforts in research and development are still required, such as to increase the C2 selectivity by mitigating CO_X formation. For decades intensive efforts have been made at different process scales emphasizing on catalysis, reactor and process design, as well as optimization of operating conditions. A promising future for OCM could come from considering that it should not go alone, but be integrated into a multi-step process, *i.e.* cascade reactors, to remove COx effluent and using it as reactant.

The MDA reaction offers the opportunity to produce dihydrogen while valorizing the carbon to hydrocarbons. Thus, from the reaction point of view, the valorization of methane occurs through a "zero" CO_2 formation path. A free carbon wasting process is not conceivable for MDA, as coke is produced, but an appropriate design of the process, involving heat management provided by renewable sources, could allow reaching a low level of CO_2 emissions.

The outlines of an MDA process can already be foreseen, but fundamental investigations are still needed, such as understanding the mechanism of methane dehydroaromatization on Mo/HZSM-5 catalysts and establishing the scheme of deactivation by coke. These are

prerequisites for designing stable and active catalysts. As for OCM, MDA technology's scale-up will need to consider the catalyst, the reactor, and the process engineering simultaneously.

Acknowledgments: This research was supported by TOTAL and Industrial Chair ANR-TOTAL “Nanocleanenergy”, the Region of Normandy (FEDER) and the Label of Excellence for the Centre for zeolites and nanoporous materials (CLEAR) supported by the Region of Normandy.

5. References

(1) *Flaring Emissions – Analysis*. IEA. https://www.iea.org/reports/flaring-emissions (accessed 2022-05-19).

(2) *Global natural gas reserves by country 2020*. Statista. https://www.statista.com/statistics/265329/countries-with-the-largest-natural-gas-reserves/ (accessed 2022-05-19).

(3) Galadima, A.; Muraza, O. Advances in Catalyst Design for the Conversion of Methane to Aromatics: A Critical Review. *Catal. Surv. Asia.* **2019**, *23* (3), 149–170. https://doi.org/10.1007/s10563-018-9262-5.

(4) Spivey, J. J.; Hutchings, G. Catalytic Aromatization of Methane. *Chem. Soc. Rev.* **2014**, *43* (3), 792–803. https://doi.org/10.1039/C3CS60259A.

(5) Ismagilov, Z. R.; Matus, E. V.; Tsikoza, L. T. Direct Conversion of Methane on Mo/ZSM-5 Catalysts to Produce Benzene and Hydrogen: Achievements and Perspectives. *Energy Environ. Sci.* **2008**, *1* (5), 526. https://doi.org/10.1039/b810981h.

(6) Vollmer, I.; Yarulina, I.; Kapteijn, F.; Gascon, J. Progress in Developing a Structure- Activity Relationship for the Direct Aromatization of Methane. *ChemCatChem* **2019**, *11* (1), 39–52. https://doi.org/10.1002/cctc.201800880.

(7) Sun, K.; Ginosar, D. M.; He, T.; Zhang, Y.; Fan, M.; Chen, R. Progress in Nonoxidative Dehydroaromatization of Methane in the Last 6 Years. *Ind. Eng. Chem. Res.* **2018**, *57* (6), 1768–1789. https://doi.org/10.1021/acs.iecr.7b04707.

(8) Kosinov, N.; Hensen, E. J. M. Reactivity, Selectivity, and Stability of Zeolite- Based Catalysts for Methane Dehydroaromatization. *Adv. Mater.* **2020**, *32* (44), 2002565. https://doi.org/10.1002/adma.202002565.

(9) Zhang, T. Recent Advances in Heterogeneous Catalysis for the Nonoxidative Conversion of Methane. *Chem. Sci.* **2021**, *12* (38), 12529–12545. https://doi.org/10.1039/D1SC02105B.

(10) Ma, S.; Guo, X.; Zhao, L.; Scott, S.; Bao, X. Recent Progress in Methane Dehydroaromatization: From Laboratory Curiosities to Promising Technology. *J. of Energy Chem.* **2013**, *22* (1), 1–20. https://doi.org/10.1016/S2095-4956(13)60001-7.

(11) Xu, Y.; Lin, L. Recent Advances in Methane Dehydro-Aromatization over Transition Metal Ion-Modified Zeolite Catalysts under Non-Oxidative Conditions. *Appl. Catal. A: Gen.* **1999**, *188* (1–2), 53–67. https://doi.org/10.1016/S0926-860X(99)00210-0.

(12) Karakaya, C.; Kee, R. J. Progress in the Direct Catalytic Conversion of Methane to Fuels and Chemicals. *Prog. Energy Combust. Sci.* **2016**, *55*, 60–97. https://doi.org/10.1016/j.pecs.2016.04.003.

(13) Nithyanandam, R.; Mun, Y. K.; Fong, T. S.; Siew, T. C.; Yee, O. S.; Ismail, N. Review on Production of Benzene from Petroleum Associated Gas by Dehydro-Aromatization, Partial Oxidation of Methane and Methanol-to-Aromatics Processes. *J. Eng. Sci. Technol.* **2018**, *13* (12), 4290–4309.

(14) Kiani, D.; Sourav, S.; Tang, Y.; Baltrusaitis, J.; E. Wachs, I. Methane Activation by ZSM-5-Supported Transition Metal Centers. *Chem. Soc. Rev.* **2021**, *50* (2), 1251–1268. https://doi.org/10.1039/D0CS01016B.

(15) Majhi, S.; Mohanty, P.; Wang, H.; Pant, K. K. Direct Conversion of Natural Gas to Higher Hydrocarbons: A Review. *J. Energy Chem.* **2013**, *22* (4), 543–554. https://doi.org/10.1016/S2095-4956(13)60071-6.

(16) Mamonov, N. A.; Fadeeva, E. V.; Grigoriev, D. A.; Mikhailov, M. N.; Kustov, L. M.; Alkhimov, S. A. Metal/Zeolite Catalysts of Methane Dehydroaromatization. *Russ. Chem. Rev.* **2013**, *82* (6), 567. https://doi.org/10.1070/RC2013v082n06ABEH004346.

(17) Xu, Y.; Bao, X.; Lin, L. Direct Conversion of Methane under Nonoxidative Conditions. *J. Catal.* **2003**, *216* (1), 386–395. https://doi.org/10.1016/S0021-9517(02)00124-0.

(18) Menon, U.; Rahman, M.; Khatib, S. J. A Critical Literature Review of the Advances in Methane Dehydroaromatization over Multifunctional Metal-Promoted Zeolite Catalysts. *Appl. Catal. A: Gen.* **2020**, *608*, 117870. https://doi.org/10.1016/j.apcata.2020.117870.

(19) Choudhary, T. V.; Aksoylu, E.; Wayne Goodman, D. Nonoxidative Activation of Methane. *Catal. Rev.* **2003**, *45* (1), 151–203. https://doi.org/10.1081/CR-120017010.

(20) Petkovic, L. M.; Ginosar, D. M. Direct Production of Hydrogen and Aromatics from Methane or Natural Gas: Review of Recent U.S. Patents. *Recent Pat. Eng. 5* (1), 2–10.

(21) Kosinov, N.; Hensen, E. J. M. Nonoxidative Dehydroaromatization of Methane. In *Nanotechnology in Catalysis*; John Wiley & Sons, Ltd, 2017; pp 469–482. https://doi.org/10.1002/9783527699827.ch20.

(22) Olivos-Suarez, A. I.; Szécsényi, À.; Hensen, E. J. M.; Ruiz-Martinez, J.; Pidko, E. A.; Gascon, J. Strategies for the Direct Catalytic Valorization of Methane Using Heterogeneous Catalysis: Challenges and Opportunities. *ACS Catal.* **2016**, *6* (5), 2965–2981. https://doi.org/10.1021/acscatal.6b00428.

(23) Ranjekar, A. M.; Yadav, G. D. Dry Reforming of Methane for Syngas Production: A Review and Assessment of Catalyst Development and Efficacy. *J. Indian Chem. Soc.* **2021**, *98* (1), 100002. https://doi.org/10.1016/j.jics.2021.100002.

(24) Lunsford, J. H. The Catalytic Oxidative Coupling of Methane. *Angew. Chem. Int. Ed. Engl.* **1995**, *34* (9), 970–980. https://doi.org/10.1002/anie.199509701.

(25) Sun, J.; Thybaut, J. W.; Marin, G. B. Microkinetics of Methane Oxidative Coupling. *Catal. Today* **2008**, *137* (1), 90–102. https://doi.org/10.1016/j.cattod.2008.02.026.

(26) Karakaya, C.; Zhu, H.; Loebick, C.; Weissman, J. G.; Kee, R. J. A Detailed Reaction Mechanism for Oxidative Coupling of Methane over Mn/Na2WO4/SiO2 Catalyst for Non-Isothermal Conditions. *Catal. Today* **2018**, *312*, 10–22. https://doi.org/10.1016/j.cattod.2018.02.023.

(27) Beck, B.; Fleischer, V.; Arndt, S.; Hevia, M. G.; Urakawa, A.; Hugo, P.; Schomäcker, R. Oxidative Coupling of Methane - A Complex Surface/Gas Phase Mechanism with Strong Impact on the Reaction Engineering. *Catal. Today* **2014**, *228*, 212–218. https://doi.org/10.1016/j.cattod.2013.11.059.

(28) Zavyalova, U.; Holena, M.; Schlögl, R.; Baerns, M. Statistical Analysis of Past Catalytic Data on Oxidative Methane Coupling for New Insights into the Composition of High-Performance Catalysts. *ChemCatChem* **2011**, *3* (12), 1935–1947. https://doi.org/10.1002/cctc.201100186.

(29) Saychu, P.; Thanasiriruk, M.; Khajonvittayakul, C.; Viratikul, R.; Tongnan, V.; Hartley, M.; Wongsakulphasatch, S.; Laosiripojana, N.; Hartley, U. W. Catalytic Performance of Na-Mn2O3-Based Catalysts towards Oxidative Coupling of Methane. *Catal. Today* **2021**, *375* (December 2019), 225–233. https://doi.org/10.1016/j.cattod.2020.12.024.

(30) Hayek, N. S.; Lucas, N. S.; Warwar Damouny, C.; Gazit, O. M. Critical Surface Parameters for the Oxidative Coupling of Methane over the Mn-Na-W/SiO2 Catalyst. *ACS Appl. Mater. Interfaces* **2017**, *9* (46), 40404–40411. https://doi.org/10.1021/acsami.7b14941.

(31) Yildiz, M.; Aksu, Y.; Simon, U.; Kailasam, K.; Goerke, O.; Rosowski, F.; Schomäcker, R.; Thomas, A.; Arndt, S. Enhanced Catalytic Performance of MnxOy–Na2WO4/SiO2 for the Oxidative Coupling of Methane Using an Ordered Mesoporous Silica Support. *Chem. Commun.* **2014**, *50* (92), 14440–14442. https://doi.org/10.1039/C4CC06561A.

(32) Sollier, B. M.; Gómez, L. E.; Boix, A. V.; Miró, E. E. Oxidative Coupling of Methane on Sr/La2O3 Catalysts: Improving the Catalytic Performance Using Cordierite Monoliths and Ceramic Foams as Structured Substrates. *Appl. Catal. A: Gen.* **2017**, *532*, 65–76. https://doi.org/10.1016/j.apcata.2016.12.018.

(33) Kim, M.; Arndt, S.; Yildiz, M.; Schomäcker, R.; Görke, O.; Repke, J.-U.; Wozny, G.; Godini, H. R. Reaction Engineering of Oxidative Coupling of Methane. *Chem. Eng. Res. Des.* **2021**, *172*, 84–98. https://doi.org/10.1016/j.cherd.2021.04.029.

(34) Noon, D.; Zohour, B.; Senkan, S. Oxidative Coupling of Methane with La2O3–CeO2 Nanofiber Fabrics: A Reaction Engineering Study. *J. Nat. Gas Sci. Eng.* **2014**, *18*, 406–411. https://doi.org/10.1016/j.jngse.2014.04.004.

(35) Langfeld, K.; Frank, B.; Strempel, V. E.; Berger-Karin, C.; Weinberg, G.; Kondratenko, E. V.; Schomäcker, R. Comparison of Oxidizing Agents for the Oxidative Coupling of Methane over State-of-the-Art Catalysts. *Appl. Catal. A: Gen.* **2012**, *417–418*, 145–152. https://doi.org/10.1016/j.apcata.2011.12.035.

(36) Roguleva, V. G.; Nikiphorova, M. A.; Maksimov, N. G.; Anshits, A. G. Oxidative Coupling of Methane over Li/CaO Catalysts Using O2 and N2O as Oxidants. *Catal. Today* **1992**, *13* (2–3), 219–226. https://doi.org/10.1016/0920-5861(92)80145-D.

(37) Yamamoto, H.; Chu, H. Y.; Xu, M. T.; Shi, C. L.; Lunsford, J. H. Oxidative Coupling of Methane over a Li+/MgO Catalyst Using N2O as an Oxidant. *J. Catal*. **1993**, 142 (1), 325–336. https://doi.org/10.1006/jcat.1993.1211.

(38) Arinaga, A. M.; Ziegelski, M. C.; Marks, T. J. Alternative Oxidants for the Catalytic Oxidative Coupling of Methane. *Angew. Chem. Int. Ed*. **2021**, *133* (19), 10596–10609. https://doi.org/10.1002/ange.202012862.

(39) Cruellas, A.; Ververs, W.; Annaland, M. van S.; Gallucci, F. Experimental Investigation of the Oxidative Coupling of Methane in a Porous Membrane Reactor: Relevance of Back-Permeation. *Membranes* **2020**, *10* (7), 152. https://doi.org/10.3390/membranes10070152.

(40) Wang, Z.; Chen, T.; Dewangan, N.; Li, Z.; Das, S.; Pati, S.; Li, Z.; Lin, J. Y. S.; Kawi, S. Catalytic Mixed Conducting Ceramic Membrane Reactors for Methane Conversion. *React. Chem. Eng.* **2020**, *5* (10), 1868–1891. https://doi.org/10.1039/d0re00177e.

(41) Han, S. J.; Kim, S. K.; Hwang, A.; Kim, S.; Hong, D.-Y.; Kwak, G.; Jun, K.-W.; Kim, Y. T. Non-Oxidative Dehydroaromatization of Methane over Mo/H-ZSM-5 Catalysts: A Detailed Analysis of the Reaction-Regeneration Cycle. *Appl. Catal. B: Environ.* **2019**, *241*, 305–318. https://doi.org/10.1016/j.apcatb.2018.09.042.

(42) Ma, H.; Kojima, R.; Ohnishi, R.; Ichikawa, M. Efficient Regeneration of Mo/HZSM-5 Catalyst by Using Air with NO in Methane Dehydro-Aromatization Reaction. *Appl. Catal. A: Gen.* **2004**, *275* (1), 183–187. https://doi.org/10.1016/j.apcata.2004.07.032.

(43) Rahman, M.; Infantes-Molina, A.; Boubnov, A.; Bare, S. R.; Stavitski, E.; Sridhar, A.; Khatib, S. J. Increasing the Catalytic Stability by Optimizing the Formation of Zeolite-Supported Mo Carbide Species Ex Situ for Methane Dehydroaromatization. *J. Catal.* **2019**, *375*, 314–328. https://doi.org/10.1016/j.jcat.2019.06.002.

(44) Tempelman, C. H. L.; Zhu, X.; Hensen, E. J. M. Activation of Mo/HZSM-5 for Methane Aromatization. *Chin. J. Catal.* **2015**, *36* (6), 829–837. https://doi.org/10.1016/S1872-2067(14)60301-6.

(45) Sridhar, A.; Rahman, M.; Infantes-Molina, A.; Wylie, B. J.; Borcik, C. G.; Khatib, S. J. Bimetallic Mo-Co/ZSM-5 and Mo-Ni/ZSM-5 Catalysts for Methane Dehydroaromatization: A Study of the Effect of Pretreatment and Metal Loadings on the Catalytic Behavior. *Appl. Catal. A: Gen.* **2020**, *589*, 117247. https://doi.org/10.1016/j.apcata.2019.117247.

(46) Tan, P. The Catalytic Performance of Mo-Impregnated HZSM-5 Zeolite in CH4 Aromatization: Strong Influence of Mo Loading and Pretreatment Conditions. *Catal. Commun.* **2018**, *103*, 101–104. https://doi.org/10.1016/j.catcom.2017.10.008.

(47) Tshabalala, T. E.; Coville, N. J.; Anderson, J. A.; Scurrell, M. S. Dehydroaromatization of Methane over Noble Metal Loaded Mo/H-ZSM-5 Zeolite Catalysts. *Appl. Petrochem. Res.* **2021**. https://doi.org/10.1007/s13203-021-00274-y.

(48) Abdelsayed, V.; Shekhawat, D.; Smith, M. W. Effect of Fe and Zn Promoters on Mo/HZSM-5 Catalyst for Methane Dehydroaromatization. *Fuel* **2015**, *139*, 401–410. https://doi.org/10.1016/j.fuel.2014.08.064.

(49) Sridhar, A.; Rahman, M.; Khatib, S. J. Enhancement of Molybdenum/ZSM-5 Catalysts in Methane Aromatization by the Addition of Iron Promoters and by

Reduction/Carburization Pretreatment. *ChemCatChem* **2018**, *10* (12), 2571–2583. https://doi.org/10.1002/cctc.201800002.

(50) Aritani, H.; Shibasaki, H.; Orihara, H.; Nakahira, A. Methane Dehydroaromatization over Mo-Modified H-MFI for Gas to Liquid Catalysts. *J. Environ. Sci.* **2009**, *21* (6), 736–740. https://doi.org/10.1016/S1001-0742(08)62333-5.

(51) Bedard, J.; Hong, D.-Y.; Bhan, A. CH4 Dehydroaromatization on Mo/H–ZSM-5: 1. Effects of Co-Processing H2 and CH3COOH. *J. Catal.* **2013**, *306*, 58–67. https://doi.org/10.1016/j.jcat.2013.06.003.

(52) Liu, S.; Dong, Q. Unique Promotion Effect of CO and CO2 on the Catalytic Stability for Benzene and Naphthalene Production from Methane on Mo/HZSM-5 Catalysts. *Chem. Commun.* **1998**, No. 11, 1217–1218. https://doi.org/10.1039/A801582A.

(53) Ohnishi, R.; Liu, S.; Dong, Q.; Wang, L.; Ichikawa, M. Catalytic Dehydrocondensation of Methane with CO and CO2 toward Benzene and Naphthalene on Mo/HZSM-5 and Fe/Co-Modified Mo/HZSM-5. *J. Catal.* **1999**, *182* (1), 92–103. https://doi.org/10.1006/jcat.1998.2319.

(54) Çağlayan, M.; Paioni, A. L.; Dereli, B.; Shterk, G.; Hita, I.; Abou-Hamad, E.; Pustovarenko, A.; Emwas, A.-H.; Dikhtiarenko, A.; Castaño, P.; Cavallo, L.; Baldus, M.; Chowdhury, A. D.; Gascon, J. Illuminating the Intrinsic Effect of Water Co-Feeding on Methane Dehydroaromatization: A Comprehensive Study. *ACS Catal.* **2021**, *11* (18), 11671–11684. https://doi.org/10.1021/acscatal.1c02763.

(55) *https://www.greencarcongress.com/2014/03/20140321-siluria.html*.

(56) Radaelli, G.; Chachra, G.; Jonnavittula, D. *Low-Energy, Low-Cost Production of Ethylene by Low- Temperature Oxidative Coupling of Methane*; Golden, CO (United States), 2017. https://doi.org/10.2172/1414280.

(57) Zurcher, F. R.; Scher, E. C.; Cizeron, J. M.; Schammel, W. P.; Tkachenko, A.; Gamoras, J.; Karshtedt, D.; Nyce, G.; RUMPLECKER, A.; McCormick, J.; Merzlyak, A.; Alcid, M.; Rosenberg, D.; Ras, E.-J. Nanowiere Catalysts and Methods for Their Use and Preparation. US 8962517 B2, 2015.

(58) Schammel, W. P.; RUMPLECKER, A.; ZURCHER, Fabio, R.; SCHER, Erik, C.; CIZERON, Joel, M.; GAMORAS, J. Heterogeneous Catalysis. Wo 2015/168601 A2, 2015.

(59) Schucker, R. C.; J. Derrickson, K.; K. Ali, A.; J. Caton, N. The Effect of Strontium Content on the Activity and Selectivity of Sr-Doped La2O3 Catalysts in Oxidative Coupling of Methane. *Appl. Catal. A: Gen.* **2020**, *607* (June), 117827. https://doi.org/10.1016/j.apcata.2020.117827.

(60) Cong, L.; Zhao, Y.; Li, S.; Sun, Y. Sr-Doping Effects on La2O3 Catalyst for Oxidative Coupling of Methane. *Chinese J. Catal.* **2017**, *38* (5), 899–907. https://doi.org/10.1016/S1872-2067(17)62823-7.

(61) Parishan, S.; Nowicka, E.; Fleischer, V.; Schulz, C.; Colmenares, M. G.; Rosowski, F.; Schomäcker, R. Investigation into Consecutive Reactions of Ethane and Ethene Under the OCM Reaction Conditions over MnxOy–Na2WO4/SiO2 Catalyst. *Catal. Lett.* **2018**, *148* (6), 1659–1675. https://doi.org/10.1007/s10562-018-2384-6.

(62) Arndt, S.; Otremba, T.; Simon, U.; Yildiz, M.; Schubert, H.; Schomäcker, R. Mn-Na 2WO 4/SiO 2 as Catalyst for the Oxidative Coupling of Methane. What Is Really Known? *Appl. Catal. A: Gen.* **2012**, *425–426*, 53–61. https://doi.org/10.1016/j.apcata.2012.02.046.

(63) Liu, W. C.; Ralston, W. T.; Melaet, G.; Somorjai, G. A. Oxidative Coupling of Methane (OCM): Effect of Noble Metal (M = Pt, Ir, Rh) Doping on the Performance of Mesoporous Silica MCF-17 Supported MnxOy-Na2WO4 Catalysts. *Appl. Catal. A: Gen.* **2017**, *545* (April), 17–23. https://doi.org/10.1016/j.apcata.2017.07.017.

(64) Sun, W.; Gao, Y.; Zhao, G.; Si, J.; Liu, Y.; Lu, Y. Mn2O3-Na2WO4 Doping of CexZr1-XO2 Enables Increased Activity and Selectivity for Low Temperature Oxidative Coupling of Methane. *J. Catal.* **2021**, *400*, 372–386. https://doi.org/10.1016/j.jcat.2021.06.027.

(65) Si, J.; Sun, W.; Zhao, G.; Lu, Y. Support Oxide Tuning of MnOx-Na2WO4 Catalysts Enables Low-Temperature Light-off of OCM. *Fuel* **2022**, *311* (October 2021), 122539. https://doi.org/10.1016/j.fuel.2021.122539.

(66) Wang, P.; Zhao, G.; Wang, Y.; Lu, Y. MnTiO 3 -Driven Low-Temperature Oxidative Coupling of Methane over TiO2 -Doped Mn2O3-Na2WO4/SiO2 Catalyst. *Sci. Adv.* **2017**, *3* (6). https://doi.org/10.1126/sciadv.1603180.

(67) Cheng, F.; Yang, J.; Yan, L.; Zhao, J.; Zhao, H.; Song, H.; Chou, L. J. Enhancement of La2O3 to Li-Mn/WO3/TiO2 for Oxidative Coupling of Methane. *J. Rare Earths* **2020**, *38* (2), 167–174. https://doi.org/10.1016/j.jre.2019.03.023.

(68) Song, J.; Sun, Y.; Ba, R.; Huang, S.; Zhao, Y.; Zhang, J.; Sun, Y.; Zhu, Y. Monodisperse Sr–La 2 O 3 Hybrid Nanofibers for Oxidative Coupling of Methane to Synthesize C 2 Hydrocarbons. *Nanoscale* **2015**, *7* (6), 2260–2264. https://doi.org/10.1039/C4NR06660J.

(69) Qian, K.; You, R.; Guan, Y.; Wen, W.; Tian, Y.; Pan, Y.; Huang, W. Single-Site Catalysis of Li-MgO Catalysts for Oxidative Coupling of Methane Reaction. *ACS Catal.* **2020**, *10* (24), 15142–15148. https://doi.org/10.1021/acscatal.0c03896.

(70) Papa, F.; Luminita, P.; Osiceanu, P.; Birjega, R.; Akane, M.; Balint, I. Acid-Base Properties of the Active Sites Responsible for C2+ and CO2 Formation over MO-Sm2O3 (M = Zn, Mg, Ca and Sr) Mixed Oxides in OCM Reaction. *J. Mol.Catal. A Chem.* **2011**, *346* (1–2), 46–54. https://doi.org/10.1016/j.molcata.2011.06.008.

(71) Feng, R.; Niu, P.; Hou, B.; Wang, Q.; Jia, L.; Lin, M.; Li, D. Synthesis and Characterization of the Flower-like LaxCe1−xO1.5+δ Catalyst for Low-Temperature Oxidative Coupling of Methane. *J. Energy Chem.* **2022**, *67*, 342–353. https://doi.org/10.1016/j.jechem.2021.10.018.

(72) Zhang, Z.; Gong, Y.; Xu, J.; Zhang, Y.; Xiao, Q.; Xi, R.; Xu, X.; Fang, X.; Wang, X. Dissecting La2Ce2O7 Catalyst to Unravel the Origin of the Surface Active Sites Devoting to Its Performance for Oxidative Coupling of Methane (OCM). *Catal. Today* **2021**, No. November. https://doi.org/10.1016/j.cattod.2021.11.012.

(73) Xi, R.; Xu, J.; Zhang, Y.; Zhang, Z.; Xu, X.; Fang, X.; Wang, X. The Enhancement Effects of BaX2 (X = F, Cl, Br) on SnO2-Based Catalysts for the Oxidative Coupling of Methane (OCM). *Catal. Today* **2021**, *364* (January 2020), 35–45. https://doi.org/10.1016/j.cattod.2020.04.010.

(74) Kwon, D.; Yang, I.; Sim, Y.; Ha, J. M.; Jung, J. C. A K2NiF4-Type La2Li0.5Al0.5O4 Catalyst for the Oxidative Coupling of Methane (OCM). *Catal. Commun.* **2019**, 128 (August 2019), https://doi.org/10.1016/j.catcom.2019.05.009.

(75) Lee, H.; Lee, D.-H.; Ha, J. M.; Kim, D. H. Plasma Assisted Oxidative Coupling of Methane (OCM) over Ag/SiO2 and Subsequent Regeneration at Low Temperature. *Appl. Catal. A: Gen.* **2018**, *557*, 39–45. https://doi.org/10.1016/j.apcata.2018.03.007.

(76) Murthy, P. R.; Liu, Y.; Wu, G.; Diao, Y.; Shi, C. Oxidative Coupling of Methane: Perspective for High-Value C2 Chemicals. *Crystals* **2021**, *11* (9). https://doi.org/10.3390/cryst11091011.

(77) Serres, T.; Aquino, C.; Mirodatos, C.; Schuurman, Y. Influence of the Composition/Texture of Mn-Na-W Catalysts on the Oxidative Coupling of Methane. *Appl. Catal. A: Gen.* **2015**, *504*, 509–518. https://doi.org/10.1016/j.apcata.2014.11.045.

(78) Wang, H.; Schmack, R.; Paul, B.; Albrecht, M.; Sokolov, S.; Rümmler, S.; Kondratenko, E. V.; Kraehnert, R. Porous Silicon Carbide as a Support for Mn/Na/W/SiC Catalyst in the Oxidative Coupling of Methane. *Appl. Catal. A: Gen.* **2017**, *537*, 33–39. https://doi.org/10.1016/j.apcata.2017.02.018.

(79) Fleischer, V.; Simon, U.; Parishan, S.; Colmenares, M. G.; Görke, O.; Gurlo, A.; Riedel, W.; Thum, L.; Schmidt, J.; Risse, T.; Dinse, K. P.; Schomäcker, R. Investigation of the Role of the Na2WO4/Mn/SiO2 Catalyst Composition in the Oxidative Coupling of Methane by Chemical Looping Experiments. *J. Catal.* **2018**, *360*, 102–117. https://doi.org/10.1016/j.jcat.2018.01.022.

(80) Palermo, A.; Vazquez, J. P. H.; Lee, A. F.; Tikhov, M. S.; Lambert, R. M. Critical Influence of the Amorphous Silica-to-Cristobalite Phase Transition on the Performance of Mn/Na2WO4/SiO2 Catalysts for the Oxidative Coupling of Methane. *J. Catal.* **1998**, *177* (2), 259–266. https://doi.org/10.1006/jcat.1998.2109.

(81) Elkins, T. W.; Hagelin-Weaver, H. E. Characterization of Mn-Na2WO4/SiO2 and Mn-Na2WO4/MgO Catalysts for the Oxidative Coupling of Methane. *Appl. Catal. A: Gen.* **2015**, *497*, 96–106. https://doi.org/10.1016/j.apcata.2015.02.040.

(82) Yildiz, M.; Aksu, Y.; Simon, U.; Otremba, T.; Kailasam, K.; Göbel, C.; Girgsdies, F.; Görke, O.; Rosowski, F.; Thomas, A.; Schomäcker, R.; Arndt, S. Silica Material Variation for the MnxOy-Na2WO4/SiO2. *Appl. Catal. A: Gen.* **2016**, *525*, 168–179. https://doi.org/10.1016/j.apcata.2016.06.034.

(83) Yıldız, M. Mesoporous TiO2-Rutile Supported MnxOy-Na2WO4: Preparation, Characterization and Catalytic Performance in the Oxidative Coupling of Methane. *J. Ind. and Eng. Chem.* **2019**, *76*, 488–499. https://doi.org/10.1016/j.jiec.2019.04.016.

(84) Matras, D.; Vamvakeros, A.; Jacques, S. D. M.; Grosjean, N.; Rollins, B.; Poulston, S.; Stenning, G. B. G.; Godini, H. R.; Drnec, J.; Cernik, R. J.; Beale, A. M. Effect of Thermal Treatment on the Stability of Na-Mn-W/SiO2catalyst for the Oxidative Coupling of Methane. *Faraday Discuss.* **2021**, *229*, 176–196. https://doi.org/10.1039/c9fd00142e.

(85) Lezcano, G.; K. Velisoju, V.; R. Kulkarni, S.; Ramirez, A.; Castaño, P. Engineering Thermally Resistant Catalytic Particles for Oxidative Coupling of Methane Using Spray-Drying and Incorporating SiC. *Ind. Eng. Chem. Res.* **2021**, *60* (51), 18770–18780. https://doi.org/10.1021/acs.iecr.1c02802.

(86) Holst, N.; Khakpour, T.; Holtappels, K.; Steinbach, J. Ignition Behavior of Methane-Oxygen Mixtures at Elevated Conditions. *AIChE Annual Meeting, Conference Proceedings* **2011**, No. 2011.

(87) Sun, Z.; West, D. H.; Gautam, P.; Balakotaiah, V. Scale-up Analysis of Autothermal Operation of Methane Oxidative Coupling with La2O3/CaO Catalyst. *AIChE Journal* **2020**, *66* (6), 1–14. https://doi.org/10.1002/aic.16949.

(88) Ching, T. T.; Mohamed, A. R.; Bhatia, S. Modeling of Catalytic Reactor for Oxidative Coupling of Methane Using La2O3/CaO Catalyst. *Chem. Eng. J.* **2002**, *87* (1), 49–59. https://doi.org/10.1016/S1385-8947(01)00191-7.

(89) Yaghobi, N. The Role of Gas Hourly Space Velocity and Feed Composition for Catalytic Oxidative Coupling of Methane: Experimental Study. *J. King Saud Univ. Eng. Sci.* **2013**, *25* (1), 1–10. https://doi.org/10.1016/j.jksues.2011.06.007.

(90) Liu, Y.; Hou, R.; Liu, X.; Xue, J.; Li, S. *Performance of Na2WO4-Mn/SiO2 Catalyst for Conversion of CH4 with CO2 into C2 Hydrocarbons and Its Mechanism*; Elsevier Masson SAS, 1998; Vol. 119. https://doi.org/10.1016/s0167-2991(98)80449-7.

(91) Zhang, X.; Dai, B.; Zhu, A.; Gong, W.; Liu, C. The Simultaneous Activation of Methane and Carbon Dioxide to C2 Hydrocarbons under Pulse Corona Plasma over La2O3/γ-Al2O3 Catalyst. *Catal. Today* **2002**, *72* (3–4), 223–227. https://doi.org/10.1016/S0920-5861(01)00496-5.

(92) Oshima, K.; Tanaka, K.; Yabe, T.; Kikuchi, E.; Sekine, Y. Oxidative Coupling of Methane Using Carbon Dioxide in an Electric Field over La-ZrO2 Catalyst at Low External Temperature. *Fuel* **2013**, *107*, 879–881. https://doi.org/10.1016/j.fuel.2013.01.058.

(93) Yoon, S.; Lim, S.; Choi, J. W.; Suh, D. J.; Song, K. H.; Ha, J. M. Study on the Unsteady State Oxidative Coupling of Methane: Effects of Oxygen Species from O2, Surface Lattice Oxygen, and CO2 on the C2+ selectivity. *RSC Adv.* **2020**, *10* (59), 35889–35897. https://doi.org/10.1039/d0ra06065h.

(94) Zhu, Q.; Wegener, S. L.; Xie, C.; Uche, O.; Neurock, M.; Marks, T. J. Sulfur as a Selective “soft” Oxidant for Catalytic Methane Conversion Probed by Experiment and Theory. *Nat. Chem.* **2013**, *5* (2), 104–109. https://doi.org/10.1038/nchem.1527.

(95) Kohl, A. L.; Nielsen, R. B. Sulfur Recovery Processes. In *Gas Purification*; Elsevier, 1997; pp 670–730. https://doi.org/10.1016/B978-088415220-0/50008-2.

(96) Williams, M. The Merck Index: An Encyclopedia of Chemicals, Drugs, and Biologicals, 15th Edition , Royal Society of Chemistry, Cambridge, ISBN 9781849736701; *Drug Development Research* **2013**.

(97) Cruellas, A.; Melchiori, T.; Gallucci, F.; van Sint Annaland, M. Oxidative Coupling of Methane: A Comparison of Different Reactor Configurations. *Energy Technol.* **2020**, *8* (8), 1–15. https://doi.org/10.1002/ente.201900148.

(98) Cruellas, A.; Heezius, J.; Spallina, V.; van Sint Annaland, M.; Medrano, J. A.; Gallucci, F. Oxidative Coupling of Methane in Membrane Reactors; A Techno-Economic Assessment. *Processes* **2020**, *8* (3), 1–25. https://doi.org/10.3390/pr8030274.

(99) Cruellas, A.; Melchiori, T.; Gallucci, F.; van Sint Annaland, M. Advanced Reactor Concepts for Oxidative Coupling of Methane. *Catal. Rev. Sci. Eng.* **2017**, *59* (3), 234–294. https://doi.org/10.1080/01614940.2017.1348085.

(100) Lei, S.; Wang, A.; Xue, J.; Wang, H. Catalytic Ceramic Oxygen Ionic Conducting Membrane Reactors for Ethylene Production. *React. Chem. Eng.* **2021**, *6* (8), 1327–1341. https://doi.org/10.1039/d1re00136a.

(101) Vandewalle, L. A.; Van de Vijver, R.; Van Geem, K. M.; Marin, G. B. The Role of Mass and Heat Transfer in the Design of Novel Reactors for Oxidative Coupling of Methane. *Chem. Eng. Sci*. **2019**, *198*, 268–289. https://doi.org/10.1016/j.ces.2018.09.022.

(102) Matras, D.; Vamvakeros, A.; Jacques, S. D. M.; Middelkoop, V.; Vaughan, G.; Agote Aran, M.; Cernik, R. J.; Beale, A. M. In Situ X-Ray Diffraction Computed Tomography Studies Examining the Thermal and Chemical Stabilities of Working Ba0.5Sr0.5Co0.8Fe0.2O3- Δmembranes during Oxidative Coupling of Methane. *Phys. Chem. Chem. Phys.* **2020**, *22* (34), 18964–18975. https://doi.org/10.1039/d0cp02144j.

(103) *Siluria by Lummus*. https://www.lummustechnology.com/Process-Technologies/Siluria.

(104) *McDermott Buys Siluria Technologies*. https://www.chemanager-online.com/en/news-opinions/headlines/mcdermott-buys-siluria-technologies.

(105) Mamedov, A.; Chang, T.; Kumar, K.; Gautam, P. Oxidative Conversion of Methane to C2 Hydrocarbons and Synthesis Gas. WO2020142594A1, July 20, 2020.

(106) *Methane oxidative conversion and hydroformylation to propylene*. https://cordis.europa.eu/project/id/814557.

(107) Wang, L.; Tao, L.; Xie, M.; Xu, G.; Huang, J.; Xu, Y. Dehydrogenation and Aromatization of Methane under Non-Oxidizing Conditions. *Catal. Lett.* **1993**, *21* (1–2), 35–41. https://doi.org/10.1007/BF00767368.

(108) Portilla, M. T.; Llopis, F. J.; Moliner, M.; Martinez, C. Influence of Preparation Conditions on the Catalytic Performance of Mo/H-ZSM-5 for Methane Dehydroaromatization. *Applied Sciences* **2021**, *11* (12), 5465. https://doi.org/10.3390/app11125465.

(109) Gao, W.; Qi, G.; Wang, Q.; Wang, W.; Li, S.; Hung, I.; Gan, Z.; Xu, J.; Deng, F. Dual Active Sites on Molybdenum/ZSM-5 Catalyst for Methane Dehydroaromatization: Insights

from Solid-State NMR Spectroscopy. *Angew. Chem. Int. Ed.* **2021**, *60* (19), 10709–10715. https://doi.org/10.1002/anie.202017074.

(110) Rahman, M.; Infantes-Molina, A.; Hoffman, A. S.; Bare, S. R.; Emerson, K. L.; Khatib, S. J. Effect of Si/Al Ratio of ZSM-5 Support on Structure and Activity of Mo Species in Methane Dehydroaromatization. *Fuel* **2020**, *278*, 118290. https://doi.org/10.1016/j.fuel.2020.118290.

(111) Tempelman, C. H. L.; de Rodrigues, V. O.; van Eck, E. R. H.; Magusin, P. C. M. M.; Hensen, E. J. M. Desilication and Silylation of Mo/HZSM-5 for Methane Dehydroaromatization. *Microporous Mesoporous Mater.* **2015**, *203*, 259–273. https://doi.org/10.1016/j.micromeso.2014.10.020.

(112) Kosinov, N.; Mezari, B.; Hensen, E. J. M. Methane Dehydroaromatization by Mo/HZSM-5: Mono- or Bifunctional Catalysis? *ACS Catal.* **2017**, 7, 520-529.https://doi.org/10.1021/acscatal.6b02497.

(113) Ramasubramanian, V.; Ramsurn, H.; Price, G. L. Methane Dehydroaromatization – A Study on Hydrogen Use for Catalyst Reduction, Role of Molybdenum, the Nature of Catalyst Support and Significance of Bronsted Acid Sites. *J. Energy Chem.* **2019**, *34*, 20–32. https://doi.org/10.1016/j.jechem.2018.09.018.

(114) Tessonnier, J.-P.; Louis, B.; Rigolet, S.; Ledoux, M. J.; Pham-Huu, C. Methane Dehydro-Aromatization on Mo/ZSM-5: About the Hidden Role of Brønsted Acid Sites. *Appl. Catal. A: Gen.* **2008**, *336* (1–2), 79–88. https://doi.org/10.1016/j.apcata.2007.08.026.

(115) Chen, M.; Song, Y.; Liu, B.; Liu, X.; Xu, Y.; Zhang, Z.-G. Experimental Investigation of the Promotion Effect of CO on Catalytic Behavior of Mo/HZSM-5 Catalyst in CH4

Dehydroaromatization at 1073 K. *Fuel* **2020**, *262*, 116674. https://doi.org/10.1016/j.fuel.2019.116674.

(116) Rahman, M.; Sridhar, A.; Khatib, S. J. Impact of the Presence of Mo Carbide Species Prepared Ex Situ in Mo/HZSM-5 on the Catalytic Properties in Methane Aromatization. *Appl. Catal. A: Gen.* **2018**, *558*, 67–80. https://doi.org/10.1016/j.apcata.2018.03.023.

(117) Martínez, A.; Peris, E. Non-Oxidative Methane Dehydroaromatization on Mo/HZSM-5 Catalysts: Tuning the Acidic and Catalytic Properties through Partial Exchange of Zeolite Protons with Alkali and Alkaline-Earth Cations. *Appl. Catal. A: Gen.* **2016**, *515*, 32–44. https://doi.org/10.1016/j.apcata.2016.01.044.

(118) Tempelman, C. H. L.; Hensen, E. J. M. On the Deactivation of Mo/HZSM-5 in the Methane Dehydroaromatization Reaction. *Appl. Catal. B: Environ.* **2015**, *176–177*, 731–739. https://doi.org/10.1016/j.apcatb.2015.04.052.

(119) Guo, X.; Fang, G.; Li, G.; Ma, H.; Fan, H.; Yu, L.; Ma, C.; Wu, X.; Deng, D.; Wei, M.; Tan, D.; Si, R.; Zhang, S.; Li, J.; Sun, L.; Tang, Z.; Pan, X.; Bao, X. Direct, Nonoxidative Conversion of Methane to Ethylene, Aromatics, and Hydrogen. *Science* **2014**, *344* (6184), 616–619. https://doi.org/10.1126/science.1253150.

(120) Bao, X.; Guo, X.; Fang, G.; Deng, D.; Ma, H.; Tan, D. Oxygen-Free Direct Conversion of Methane and Catalysts Therefor. US20180169621A1, June 21, 2018.

(121) Xie, P.; Pu, T.; Nie, A.; Hwang, S.; Purdy, S. C.; Yu, W.; Su, D.; Miller, J. T.; Wang, C. Nanoceria-Supported Single-Atom Platinum Catalysts for Direct Methane Conversion. *ACS Catal.* **2018**, *8* (5), 4044–4048. https://doi.org/10.1021/acscatal.8b00004.

(122) Puente-Urbina, A.; Pan, Z.; Paunović, V.; Šot, P.; Hemberger, P.; van Bokhoven, J. A. Direct Evidence on the Mechanism of Methane Conversion under Non-Oxidative Conditions

over Iron-Modified Silica: The Role of Propargyl Radicals Unveiled. *Angew. Chem., Int. Ed. Engl.* **2021**, *60* (45), 24002–24007. https://doi.org/10.1002/anie.202107553.

(123) Toraman, H. E.; Alexopoulos, K.; Oh, S. C.; Cheng, S.; Liu, D.; Vlachos, D. G. Ethylene Production by Direct Conversion of Methane over Isolated Single Active Centers. *Chem. Eng. J.* **2021**, *420*, 130493. https://doi.org/10.1016/j.cej.2021.130493.

(124) Gu, Y.; Chen, P.; Wang, X.; Lyu, Y.; Liu, W.; Liu, X.; Yan, Z. Active Sites and Induction Period of Fe/ZSM-5 Catalyst in Methane Dehydroaromatization. *ACS Catal.* **2021**, 6771–6786. https://doi.org/10.1021/acscatal.1c01467.

(125) Tan, P. Active Phase, Catalytic Activity, and Induction Period of Fe/Zeolite Material in Nonoxidative Aromatization of Methane. *J. Catal.* **2016**, *338*, 21–29. https://doi.org/10.1016/j.jcat.2016.01.027.

(126) Xu, Y.; Yuan, X.; Chen, M.; Dong, A.; Liu, B.; Jiang, F.; Yang, S.; Liu, X. Identification of Atomically Dispersed Fe-Oxo Species as New Active Sites in HZSM-5 for Efficient Non-Oxidative Methane Dehydroaromatization. *J. Catal.* **2021**, *396*, 224–241. https://doi.org/10.1016/j.jcat.2021.02.028.

(127) Lai, Y.; Veser, G. The Nature of the Selective Species in Fe-HZSM-5 for Non-Oxidative Methane Dehydroaromatization. *Catal. Sci. Technol.* **2016**, *6* (14), 5440–5452. https://doi.org/10.1039/C5CY02258D.

(128) Sim, J. P.; Lee, B. J.; Han, G.-H.; Kim, D. H.; Lee, K.-Y. Promotional Effect of Au on Fe/HZSM-5 Catalyst for Methane Dehydroaromatization. *Fuel* **2020**, *274*, 117852. https://doi.org/10.1016/j.fuel.2020.117852.

(129) Han, S. J.; Lee, S. W.; Kim, H. W.; Kim, S. K.; Kim, Y. T. Nonoxidative Direct Conversion of Methane on Silica-Based Iron Catalysts: Effect of Catalytic Surface. *ACS Catal.* **2019**, *9* (9), 7984–7997. https://doi.org/10.1021/acscatal.9b01643.

(130) Dutta, K.; Shahryari, M.; Kopyscinski, J. Direct Nonoxidative Methane Coupling to Ethylene over Gallium Nitride: A Catalyst Regeneration Study. *Ind. Eng. Chem. Res.* **2020**, *59* (10), 4245–4256. https://doi.org/10.1021/acs.iecr.9b05548.

(131) Dutta, K.; Chaudhari, V.; Li, C.-J.; Kopyscinski, J. Methane Conversion to Ethylene over GaN Catalysts. Effect of Catalyst Nitridation. *Appl. Catal. A: Gen.* **2020**, *595*, 117430. https://doi.org/10.1016/j.apcata.2020.117430.

(132) Soulivong, D.; Norsic, S.; Taoufik, M.; Coperet, C.; Thivolle-Cazat, J.; Chakka, S.; Basset, J.-M. Non-Oxidative Coupling Reaction of Methane to Ethane and Hydrogen Catalyzed by the Silica-Supported Tantalum Hydride: (≡SiO)2Ta−H. *J. Am. Chem. Soc.* **2008**, *130* (15), 5044–5045. https://doi.org/10.1021/ja800863x.

(133) Xiao, Y.; Varma, A. Highly Selective Nonoxidative Coupling of Methane over Pt-Bi Bimetallic Catalysts. *ACS Catal.* **2018**, *8* (4), 2735–2740. https://doi.org/10.1021/acscatal.8b00156.

(134) Gerceker, D.; Motagamwala, A. H.; Rivera-Dones, K. R.; Miller, J. B.; Huber, G. W.; Mavrikakis, M.; Dumesic, J. A. Methane Conversion to Ethylene and Aromatics on PtSn Catalysts. *ACS Catal.* **2017**, *7* (3), 2088–2100. https://doi.org/10.1021/acscatal.6b02724.

(135) López-Martín, A.; Sini, M. F.; Cutrufello, M. G.; Caballero, A.; Colón, G. Characterization of Re-Mo/ZSM-5 Catalysts: How Re Improves the Performance of Mo in the Methane Dehydroaromatization Reaction. *Appl. Catal. B: Environ.* **2022**, *304*, 120960. https://doi.org/10.1016/j.apcatb.2021.120960.

(136) Nam, K.; Ryu, H. W.; Gim, M. Y.; Kim, D. H. Enhanced Reactivity and Stability in Methane Dehydro-Aromatization over Mo/HZSM-5 Physically Mixed with NiO. *Appl. Catal. B: Environ.* **2021**, *296*, 120377. https://doi.org/10.1016/j.apcatb.2021.120377.

(137) Aboul-Gheit, A. K.; Awadallah, A. E.; Aboul-Enein, A. A.; Mahmoud, A.-L. H. Molybdenum Substitution by Copper or Zinc in H-ZSM-5 Zeolite for Catalyzing the Direct Conversion of Natural Gas to Petrochemicals under Non-Oxidative Conditions. *Fuel* **2011**, *90* (10), 3040–3046. https://doi.org/10.1016/j.fuel.2011.05.010.

(138) Tshabalala, T. E.; Coville, N. J.; Scurrell, M. S. Dehydroaromatization of Methane over Doped Pt/Mo/H-ZSM-5 Zeolite Catalysts: The Promotional Effect of Tin. *Appl. Catal. A: Gen.* **2014**, *485*, 238–244. https://doi.org/10.1016/j.apcata.2014.07.022.

(139) Aboul-Gheit, A. K.; El-Masry, M. S.; Awadallah, A. E. Oxygen Free Conversion of Natural Gas to Useful Hydrocarbons and Hydrogen over Monometallic Mo and Bimetallic Mo–Fe, Mo–Co or Mo–Ni/HZSM-5 Catalysts Prepared by Mechanical Mixing. *Fuel Process. Technol.* **2012**, *102*, 24–29. https://doi.org/10.1016/j.fuproc.2012.04.017.

(140) Kosinov, N.; Coumans, F. J. A. G.; Li, G.; Uslamin, E.; Mezari, B.; Wijpkema, A. S. G.; Pidko, E. A.; Hensen, E. J. M. Stable Mo/HZSM-5 Methane Dehydroaromatization Catalysts Optimized for High-Temperature Calcination-Regeneration. *J. Catal.* **2017**, *346*, 125–133. https://doi.org/10.1016/j.jcat.2016.12.006.

(141) Vollmer, I.; Li, G.; Yarulina, I.; Kosinov, N.; Hensen, E. J.; Houben, K.; Mance, D.; Baldus, M.; Gascon, J.; Kapteijn, F. Relevance of the Mo-Precursor State in H-ZSM-5 for Methane Dehydroaromatization. *Catal. Sci. Technol.* **2018**, *8* (3), 916–922. https://doi.org/10.1039/C7CY01789H.

(142) Gu, Y.; Chen, P.; Yan, H.; Wang, X.; Lyu, Y.; Tian, Y.; Liu, W.; Yan, Z.; Liu, X. Coking Mechanism of Mo/ZSM-5 Catalyst in Methane Dehydroaromatization. *Appl. Catal. A: Gen.* **2021**, *613*, 118019. https://doi.org/10.1016/j.apcata.2021.118019.

(143) Çağlayan, M.; Paioni, A. L.; Abou- Hamad, E.; Shterk, G.; Pustovarenko, A.; Baldus, M.; Chowdhury, A. D.; Gascon, J. Initial Carbon−Carbon Bond Formation during the Early Stages of Methane Dehydroaromatization. *Angew. Chem. Int. Ed.* **2020**, *59* (38), 16741–16746. https://doi.org/10.1002/anie.202007283.

(144) Portilla, M. T.; Llopis, F. J.; Martínez, C. Non-Oxidative Dehydroaromatization of Methane: An Effective Reaction–Regeneration Cyclic Operation for Catalyst Life Extension. *Catal. Sci. Technol.* **2015**, *5* (7), 3806–3821. https://doi.org/10.1039/C5CY00356C.

(145) Ramirez-Mendoza, H.; Valdez Lancinha Pereira, M.; Van Gerven, T.; Lutz, C.; Julian, I. Ultrasound-Assisted Preparation of Mo/ZSM-5 Zeolite Catalyst for Non-Oxidative Methane Dehydroaromatization. *Catalysts* **2021**, *11* (3), 313. https://doi.org/10.3390/catal11030313.

(146) Julian, I.; Roedern, M. B.; Hueso, J. L.; Irusta, S.; Baden, A. K.; Mallada, R.; Davis, Z.; Santamaria, J. Supercritical Solvothermal Synthesis under Reducing Conditions to Increase Stability and Durability of Mo/ZSM-5 Catalysts in Methane Dehydroaromatization. *Appl. Catal. B: Environ.* **2020**, *263*, 118360. https://doi.org/10.1016/j.apcatb.2019.118360.

(147) Konnov, S. V.; Dubray, F.; Clatworthy, E. B.; Kouvatas, C.; Gilson, J.-P.; Dath, J.-P.; Minoux, D.; Aquino, C.; Valtchev, V.; Moldovan, S.; Koneti, S.; Nesterenko, N.; Mintova, S. Novel Strategy for the Synthesis of Ultra-Stable Single-Site Mo-ZSM-5 Zeolite Nanocrystals. *Angew. Chem. Int. Ed.* **2020**, *59* (44), 19553–19560. https://doi.org/10.1002/anie.202006524.

(148) Hu, J.; Wu, S.; Liu, H.; Ding, H.; Li, Z.; Guan, J.; Kan, Q. Effect of Mesopore Structure of TNU-9 on Methane Dehydroaromatization. *RSC Adv.* **2014**, *4* (51), 26577–26584. https://doi.org/10.1039/C4RA03945A.

(149) Liu, H.; Yang, S.; Wu, S.; Shang, F.; Yu, X.; Xu, C.; Guan, J.; Kan, Q. Synthesis of Mo/TNU-9 (TNU-9 Taejon National University No. 9) Catalyst and Its Catalytic Performance in Methane Non-Oxidative Aromatization. *Energy* **2011**, *36* (3), 1582–1589. https://doi.org/10.1016/j.energy.2010.12.073.

(150) Liu, H.; Wu, S.; Guo, Y.; Shang, F.; Yu, X.; Ma, Y.; Xu, C.; Guan, J.; Kan, Q. Synthesis of Mo/IM-5 Catalyst and Its Catalytic Behavior in Methane Non-Oxidative Aromatization. *Fuel* **2011**, *90* (4), 1515–1521. https://doi.org/10.1016/j.fuel.2010.11.027.

(151) Liu, H.; Zhou, C.; Zhang, Y.; Kan, Q. Facile Preparation of Hierarchically Porous IM-5 Zeolite with Enhanced Catalytic Performance in Methane Aromatization. *J. Fuel Chem. Technol.* **2017**, *45* (9), 1074–1081. https://doi.org/10.1016/S1872-5813(17)30049-X.

(152) Martínez, A.; Peris, E.; Sastre, G. Dehydroaromatization of Methane under Non-Oxidative Conditions over Bifunctional Mo/ITQ-2 Catalysts. *Catal. Today* **2005**, *107–108*, 676–684. https://doi.org/10.1016/j.cattod.2005.07.051.

(153) Jin, Z.; Liu, S.; Qin, L.; Liu, Z.; Wang, Y.; Xie, Z.; Wang, X. Methane Dehydroaromatization by Mo-Supported MFI-Type Zeolite with Core–Shell Structure. *Appl. Catal. A: Gen.* **2013**, *453*, 295–301. https://doi.org/10.1016/j.apcata.2012.12.043.

(154) Kanitkar, S.; Abedin, M. A.; Bhattar, S.; Spivey, J. J. Methane Dehydroaromatization over Molybdenum Supported on Sulfated Zirconia Catalysts. *Appl. Catal. A: Gen.* **2019**, *575*, 25–37. https://doi.org/10.1016/j.apcata.2019.01.013.

(155) Schwach, P.; Pan, X.; Bao, X. Direct Conversion of Methane to Value-Added Chemicals over Heterogeneous Catalysts: Challenges and Prospects. *Chem. Rev.* **2017**, *117* (13), 8497–8520. https://doi.org/10.1021/acs.chemrev.6b00715.

(156) Kosinov, N.; Wijpkema, A. S. G.; Uslamin, E.; Rohling, R.; Coumans, F. J. A. G.; Mezari, B.; Parastaev, A.; Poryvaev, A. S.; Fedin, M. V.; Pidko, E. A.; Hensen, E. J. M. Confined Carbon Mediating Dehydroaromatization of Methane over Mo/ZSM-5. *Angew. Chem. Int. Ed.* **2018**, *57* (4), 1016–1020. https://doi.org/10.1002/anie.201711098.

(157) Gao, J.; Zheng, Y.; Jehng, J.-M.; Tang, Y.; Wachs, I. E.; Podkolzin, S. G. Identification of Molybdenum Oxide Nanostructures on Zeolites for Natural Gas Conversion. *Science* **2015**, *348* (6235), 686–690. https://doi.org/10.1126/science.aaa7048.

(158) Vollmer, I.; van der Linden, B.; Ould-Chikh, S.; Aguilar-Tapia, A.; Yarulina, I.; Abou-Hamad, E.; Sneider, Y. G.; Olivos Suarez, A. I.; Hazemann, J.-L.; Kapteijn, F.; Gascon, J. On the Dynamic Nature of Mo Sites for Methane Dehydroaromatization. *Chem. Sci.* **2018**, *9* (21), 4801–4807. https://doi.org/10.1039/C8SC01263F.

(159) Solymosi, F.; Szöke, A.; Cserényi, J. Conversion of Methane to Benzene over Mo2C and Mo2C/ZSM-5 Catalysts. *Catal. Lett.* **1996**, *39* (3–4), 157–161. https://doi.org/10.1007/BF00805576.

(160) Weckhuysen, B. M.; Rosynek, M. P.; Lunsford, J. H. Characterization of Surface Carbon Formed during the Conversion of Methane to Benzene over Mo/H-ZSM-5 Catalysts. *Catal. Lett.* **1998**, *52* (1), 31–36. https://doi.org/10.1023/A:1019094630691.

(161) Solymosi, F.; Erdöhelyi, A.; Szöke, A. Dehydrogenation of Methane on Supported Molybdenum Oxides. Formation of Benzene from Methane. *Catal. Lett.* **1995**, *32* (1), 43–53. https://doi.org/10.1007/BF00806100.

(162) Liu, H.; Shen, W.; Bao, X.; Xu, Y. Identification of Mo Active Species for Methane Dehydro-Aromatization over Mo/HZSM-5 Catalysts in the Absence of Oxygen: 1H MAS NMR and EPR Investigations. *J. Mol. Catal. A Chem.* **2006**, *244* (1), 229–236. https://doi.org/10.1016/j.molcata.2005.09.006.

(163) Agote- Arán, M.; Kroner, A. B.; Islam, H. U.; Sławiński, W. A.; Wragg, D. S.; Lezcano- González, I.; Beale, A. M. Determination of Molybdenum Species Evolution during Non- Oxidative Dehydroaromatization of Methane and Its Implications for Catalytic Performance. *ChemCatChem* **2019**, *11* (1), 473–480. https://doi.org/10.1002/cctc.201801299.

(164) Lezcano-González, I.; Oord, R.; Rovezzi, M.; Glatzel, P.; Botchway, S. W.; Weckhuysen, B. M.; Beale, A. M. Molybdenum Speciation and Its Impact on Catalytic Activity during Methane Dehydroaromatization in Zeolite ZSM-5 as Revealed by Operando X-Ray Methods. *Angew. Chem. Int. Ed.* **2016**, *55* (17), 5215–5219. https://doi.org/10.1002/anie.201601357.

(165) Li, G.; Vollmer, I.; Liu, C.; Gascon, J.; Pidko, E. A. Structure and Reactivity of the Mo/ZSM-5 Dehydroaromatization Catalyst: An Operando Computational Study. *ACS Catal.* **2019**, *9* (9), 8731–8737. https://doi.org/10.1021/acscatal.9b02213.

(166) Borry, R. W.; Kim, Y. H.; Huffsmith, A.; Reimer, J. A.; Iglesia, E. Structure and Density of Mo and Acid Sites in Mo-Exchanged H-ZSM5 Catalysts for Nonoxidative Methane Conversion. *J. Phys. Chem. B* **1999**, *103* (28), 5787–5796. https://doi.org/10.1021/jp990866v.

(167) Beuque, A.; Hao, H.; Berrier, E.; Batalha, N.; Sachse, A.; Paul, J.-F.; Pinard, L. How Do the Products in Methane Dehydroaromatization Impact the Distinct Stages of the

Reaction? *Appl. Catal. B: Environ.* **2022**, *309*, 121274. https://doi.org/10.1016/j.apcatb.2022.121274.

(168) Kosinov, N.; Uslamin, E. A.; Coumans, F. J. A. G.; Wijpkema, A. S. G.; Rohling, R. Y.; Hensen, E. J. M. Structure and Evolution of Confined Carbon Species during Methane Dehydroaromatization over Mo/ZSM-5. *ACS Catal.* **2018**, *8* (9), 8459–8467. https://doi.org/10.1021/acscatal.8b02491.

(169) Vollmer, I.; Kosinov, N.; Szécsényi, Á.; Li, G.; Yarulina, I.; Abou-Hamad, E.; Gurinov, A.; Ould-Chikh, S.; Aguilar-Tapia, A.; Hazemann, J.-L.; Pidko, E.; Hensen, E.; Kapteijn, F.; Gascon, J. A Site-Sensitive Quasi-in Situ Strategy to Characterize Mo/HZSM-5 during Activation. *J. Catal.* **2019**, *370*, 321–331. https://doi.org/10.1016/j.jcat.2019.01.013.

(170) Ma, D.; Shu, Y.; Cheng, M.; Xu, Y.; Bao, X. On the Induction Period of Methane Aromatization over Mo-Based Catalysts. *J. Catal.* **2000**, *194* (1), 105–114. https://doi.org/10.1006/jcat.2000.2908.

(171) Hu, J.; Liu, J.; Liu, J.; Li, Y.; Li, P.; Wang, Y.; Guan, J.; Kan, Q. Enhancing Methane Aromatization Performance by Reducing the Particle Size of Molybdenum Oxide. *Nanomaterials* **2020**, *10* (10), 1991. https://doi.org/10.3390/nano10101991.

(172) Zhao, K.; Jia, L.; Wang, J.; Hou, B.; Li, D. The Influence of the Si/Al Ratio of Mo/HZSM-5 on Methane Non-Oxidative Dehydroaromatization. *New J. Chem.* **2019**, *43* (10), 4130–4136. https://doi.org/10.1039/C9NJ00114J.

(173) Agote- Arán, M.; Fletcher, R. E.; Briceno, M.; Kroner, A. B.; Sazanovich, I. V.; Slater, B.; Rivas, M. E.; Smith, A. W. J.; Collier, P.; Lezcano- González, I.; Beale, A. M. Implications of the Molybdenum Coordination Environment in MFI Zeolites on Methane

Dehydroaromatisation Performance. *ChemCatChem* **2020**, *12* (1), 294–304. https://doi.org/10.1002/cctc.201901166.

(174) Gao, J.; Zheng, Y.; Fitzgerald, G. B.; de Joannis, J.; Tang, Y.; Wachs, I. E.; Podkolzin, S. G. Structure of Mo2Cx and Mo4Cx Molybdenum Carbide Nanoparticles and Their Anchoring Sites on ZSM-5 Zeolites. *J. Phys. Chem. C* **2014**, *118* (9), 4670–4679. https://doi.org/10.1021/jp4106053.

(175) Song, Y.; Xu, Y.; Suzuki, Y.; Nakagome, H.; Ma, X.; Zhang, Z.-G. The Distribution of Coke Formed over a Multilayer Mo/HZSM-5 Fixed Bed in H2 Co-Fed Methane Aromatization at 1073 K: Exploration of the Coking Pathway. *J. Catal.* **2015**, *330*, 261–272. https://doi.org/10.1016/j.jcat.2015.07.017.

(176) Matus, E. V.; Ismagilov, I. Z.; Sukhova, O. B.; Zaikovskii, V. I.; Tsikoza, L. T.; Ismagilov, Z. R.; Moulijn, J. A. Study of Methane Dehydroaromatization on Impregnated Mo/ZSM-5 Catalysts and Characterization of Nanostructured Molybdenum Phases and Carbonaceous Deposits. *Ind. Eng. Chem. Res.* **2007**, *46* (12), 4063–4074. https://doi.org/10.1021/ie0609564.

(177) Ma, D.; Wang, D.; Su, L.; Shu, Y.; Xu, Y.; Bao, X. Carbonaceous Deposition on Mo/HMCM-22 Catalysts for Methane Aromatization: A TP Technique Investigation. *J. Catal.* **2002**, *208* (2), 260–269. https://doi.org/10.1006/jcat.2002.3540.

(178) Leary, K. J.; Michaels, J. N.; Stacy, A. M. Carbon and Oxygen Atom Mobility during Activation of Mo2C Catalysts. *J. Catal.* **1986**, *101* (2), 301–313. https://doi.org/10.1016/0021-9517(86)90257-5.

(179) Ding, W.; Meitzner, G. D.; Iglesia, E. The Effects of Silanation of External Acid Sites on the Structure and Catalytic Behavior of Mo/H–ZSM5. *J. Catal.* **2002**, *206* (1), 14–22. https://doi.org/10.1006/jcat.2001.3457.

(180) Ma, D.; Lu, Y.; Su, L.; Xu, Z.; Tian, Z.; Xu, Y.; Lin, L.; Bao, X. Remarkable Improvement on the Methane Aromatization Reaction: A Highly Selective and Coking-Resistant Catalyst. *J. Phys. Chem. B* **2002**, *106* (34), 8524–8530. https://doi.org/10.1021/jp020166h.

(181) Song, Y.; Xu, Y.; Suzuki, Y.; Nakagome, H.; Zhang, Z.-G. A Clue to Exploration of the Pathway of Coke Formation on Mo/HZSM-5 Catalyst in the Non-Oxidative Methane Dehydroaromatization at 1073K. *Appl. Catal. A: Gen.* **2014**, *482*, 387–396. https://doi.org/10.1016/j.apcata.2014.06.018.

(182) Muradov, N.; Smith, F.; T-Raissi, A. Catalytic Activity of Carbons for Methane Decomposition Reaction. *Catal. Today* **2005**, *102–103*, 225–233. https://doi.org/10.1016/j.cattod.2005.02.018.

(183) Jana, S. K.; Kotta Varithottil, Z.; Dubey, V.; Rao, G. S.; Sivakumar, S. Improved Protocol for Optimizing Mo/ZSM-5 Catalyst for Methane Aromatization. *Mol. Catal.* **2021**, *515*, 111875. https://doi.org/10.1016/j.mcat.2021.111875.

(184) Wu, Y.; Emdadi, L.; Oh, S. C.; Sakbodin, M.; Liu, D. Spatial Distribution and Catalytic Performance of Metal–Acid Sites in Mo/MFI Catalysts with Tunable Meso-/Microporous Lamellar Zeolite Structures. *J. Catal.* **2015**, *323*, 100–111. https://doi.org/10.1016/j.jcat.2014.12.022.

(185) Shu, Y.; Ma, H.; Ohnishi, R.; Ichikawa, M. Highly Stable Performance of Catalytic Methane Dehydrocondensation towards Benzene on Mo/HZSM-5 by a Periodic Switching

Treatment with H2 and CO2. *Chem. Commun.* **2003**, *0* (1), 86–87. https://doi.org/10.1039/B208607G.

(186) Larachi, F.; Oudghiri-Hassani, H.; Iliuta, M. C.; Grandjean, B. P. A.; McBreen, P. H. Ru-Mo/HZSM-5 Catalyzed Methane Aromatization in Membrane Reactors. *Catal. Lett.* **2002**, *84* (3), 183–192. https://doi.org/10.1023/A:1021475819517.

(187) Wong, K. S.; Thybaut, J. W.; Tangstad, E. Methane Aromatisation Based upon Elementary Steps: Kinetic and Catalyst Descriptors. *Microporous and Mesoporous Mater.* **2012**, *164*, 302–312.https://doi.org/10.1016/j.micromeso.2012.07.002.

(188) Ma, H.; Kojima, R.; Kikuchi, S.; Ichikawa, M. Hydrogen Effect on Coke Removal and Catalytic Performance in Pre-Carburization and Methane Dehydro-Aromatization Reaction on Mo/HZSM-5. *J. Nat. Gas Chem.* **2005**, *14* (3), 11.

(189) Vollmer, I.; Mondal, A.; Yarulina, I.; Abou-Hamad, E.; Kapteijn, F.; Gascon, J. Quantifying the Impact of Dispersion, Acidity and Porosity of Mo/HZSM-5 on the Performance in Methane Dehydroaromatization. *Appl. Catal. A: Gen.* **2019**, *574*, 144–150. https://doi.org/10.1016/j.apcata.2019.01.022.

(190) Liu, B. S.; Jiang, L.; Sun, H.; Au, C. T. XPS, XAES, and TG/DTA Characterization of Deposited Carbon in Methane Dehydroaromatization over Ga–Mo/ZSM-5 Catalyst. *Appl. Surf. Sci.* **2007**, *253* (11), 5092–5100. https://doi.org/10.1016/j.apsusc.2006.11.031.

(191) Luo, M.; Zang, H.; Hu, B.; Wang, B.; Mao, G. Evolution of Confined Species and Their Effects on Catalyst Deactivation and Olefin Selectivity in SAPO-34 Catalyzed MTO Process. *RSC Adv.* **2016**, *6* (21), 17651–17658. https://doi.org/10.1039/C5RA22424A.

(192) Magnoux, P.; Guisnet, M. Coking, Aging, and Regeneration of Zeolites: X-Nature of Coke Formed on H-Erionite during n-Heptane Cracking, Mode of Deactivation. *Zeolites* **1989**, *9* (4), 329–335. https://doi.org/10.1016/0144-2449(89)90080-8.

(193) Hamieh, S.; Canaff, C.; Tayeb, K. B.; Tarighi, M.; Maury, S.; Vezin, H.; Pouilloux, Y.; Pinard, L. Methanol and Ethanol Conversion into Hydrocarbons over H-ZSM-5 Catalyst. *Eur. Phys. J. Spec. Top.* **2015**, *224* (9), 1817–1830. https://doi.org/10.1140/epjst/e2015-02501-1.

(194) *Handbook of Petroleum Processing*; Treese, S. A., Pujadó, P. R., Jones, D. S. J., Eds.; Springer International Publishing: Cham, 2015. https://doi.org/10.1007/978-3-319-14529-7.

(195) Zheng, H.; Ma, D.; Bao, X.; Hu, J. Z.; Kwak, J. H.; Wang, Y.; Peden, C. H. F. Direct Observation of the Active Center for Methane Dehydroaromatization Using an Ultrahigh Field 95Mo NMR Spectroscopy. *J. Am. Chem. Soc.* **2008**, *130* (12), 3722–3723. https://doi.org/10.1021/ja7110916.

(196) Chung, S. Y.; Kim, B. S.; Hong, S. B.; Nam, I.-S.; Kim, Y. G. Effect of Si/Al Ratio of Mordenite and ZSM5 Type Zeolite Catalysts on Hydrothermal Stability for NO Reduction by Hydrocarbons. In *Studies in Surface Science and Catalysis*; Corma, A., Melo, F. V., Mendioroz, S., Fierro, J. L. G., Eds.; 12th International Congress on Catalysis; Elsevier, 2000; Vol. 130, pp 1511–1516. https://doi.org/10.1016/S0167-2991(00)80414-0.

(197) Cruciani, G. Zeolites upon Heating: Factors Governing Their Thermal Stability and Structural Changes. *J. Phys. Chem. Solids* **2006**, *67* (9), 1973–1994. https://doi.org/10.1016/j.jpcs.2006.05.057.

(198) Dubray, F.; Moldovan, S.; Kouvatas, C.; Grand, J.; Aquino, C.; Barrier, N.; Gilson, J.-P.; Nesterenko, N.; Minoux, D.; Mintova, S. Direct Evidence for Single Molybdenum Atoms

Incorporated in the Framework of MFI Zeolite Nanocrystals. *J. Am. Chem. Soc.* **2019**, *141* (22), 8689–8693. https://doi.org/10.1021/jacs.9b02589.

(199) Dubray, F.; Dib, E.; Medeiros-Costa, I.; Aquino, C.; Minoux, D.; Daele, S. van; Nesterenko, N.; Gilson, J.-P.; Mintova, S. The Challenge of Silanol Species Characterization in Zeolites. *Inorg. Chem. Front.* **2022**. https://doi.org/10.1039/D1QI01483H.

(200) Medeiros-Costa, I. C.; Dib, E.; Dubray, F.; Moldovan, S.; Gilson, J.-P.; Dath, J.-P.; Nesterenko, N.; Aleksandrov, H. A.; Vayssilov, G. N.; Mintova, S. Unraveling the Effect of Silanol Defects on the Insertion of Single-Site Mo in the MFI Zeolite Framework. *Inorg. Chem.* **2022**, *61* (3), 1418–1425. https://doi.org/10.1021/acs.inorgchem.1c03076.

(201) Lacheen, H.; Iglesia, E. Stability, Structure, and Oxidation State of Mo/H-ZSM-5 Catalysts during Reactions of CH4 and CH4–CO2 Mixtures. *J. Catal.* **2005**, *230* (1), 173–185. https://doi.org/10.1016/j.jcat.2004.11.037.

(202) Li, B.; Li, S.; Li, N.; Chen, H.; Zhang, W.; Bao, X.; Lin, B. Structure and Acidity of Mo/ZSM-5 Synthesized by Solid State Reaction for Methane Dehydrogenation and Aromatization. *Microporous and Mesoporous Mater.* **2006**, *88* (1), 244–253. https://doi.org/10.1016/j.micromeso.2005.09.016.

(203) Weckhuysen, B. M.; Wang, D.; Rosynek, M. P.; Lunsford, J. H. Conversion of Methane to Benzene over Transition Metal Ion ZSM-5 Zeolites: I. Catalytic Characterization. *J. Catal.* **1998**, *175* (2), 338–346. https://doi.org/10.1006/jcat.1998.2010.

(204) Xu, Y.; Song, Y.; Suzuki, Y. Effect of Superficial Velocity on the Coking Behavior of a Nanozeolite-Based Mo/HZSM-5 Catalyst in the Non-Oxidative CH4 Dehydroaromatization at 1073 K. *Catal. Sci. Technol.* **2013**, *3*, 2769–2777. https://doi.org/10.1039/C3CY00320E.

(205) Moghimpour Bijani, P.; Sohrabi, M.; Sahebdelfar, S. Thermodynamic Analysis of Nonoxidative Dehydroaromatization of Methane. *Chem. Eng. Technol.* **2012**, *35* (10), 1825–1832. https://doi.org/10.1002/ceat.201100436.

(206) Matus, E. V.; Sukhova, O. B.; Ismagilo, I. Z; Zaikovski, V. I.; Kerzhentse, M. A; Ismagilov, Z. R.; Dosumov, K. D; Mustafi, A. G. Deactivation and Regeneration of Mo/ZSM-5 Catalysts for Methane Dehydroaromatization. *Eurasian Chem.-Technol. J.* **2010**, *12*, 1–8. https://doi.org/10.18321/ectj19.

(207) Perot, G.; Guisnet, M. Advantages and Disadvantages of Zeolites as Catalysts in Organic Chemistry. *J. Mol. Catal.* **1990**, *61* (2), 173–196. https://doi.org/10.1016/0304-5102(90)85154-A.

(208) Kosinov, N.; Hensen, E. J. M.; Liu, Y. Reversible Nature of Coke Formation on Mo/ZSM- 5 Methane Dehydroaromatization Catalysts. *Angew. Chem., Int. Ed. Engl.* **2019**, *58* (21), 7068–7072. https://doi.org/10.1002/anie.201902730.

(209) Liu, Y.; Zhang, H.; Wijpkema, A. S. G.; Coumans, F. J. A. G.; Meng, L.; Uslamin, E. A.; Longo, A.; Hensen, E. J. M.; Kosinov, N. Understanding the Preparation and Reactivity of Mo/ZSM-5 Methane Dehydroaromatization Catalysts. *Chem. Eur. J.* **2022**, *28* (5), e202103894. https://doi.org/10.1002/chem.202103894.

(210) Lu, Y.; Xu, Z.; Tian, Z.; Zhang, T.; Lin, L. Methane Aromatization in the Absence of an Added Oxidant and the Bench Scale Reaction Test. *Catal. Lett.* **1999**, *62* (2), 215–220. https://doi.org/10.1023/A:1019063425801.

(211) Kim, Y.-H.; Borry, R. W.; Iglesia, E. Genesis of Methane Activation Sites in Mo-Exchanged H–ZSM-5 Catalysts. *Microporous Mesoporous Mater.* **2000**, *35–36*, 495–509. https://doi.org/10.1016/S1387-1811(99)00245-0.

(212) Cerqueira, H. S.; Caeiro, G.; Costa, L.; Ramôa Ribeiro, F. Deactivation of FCC Catalysts. *J. Mol. Catal. A Chem.* **2008**, *292* (1), 1–13. https://doi.org/10.1016/j.molcata.2008.06.014.

(213) Kosinov, N.; Coumans, F. J. A. G.; Uslamin, E.; Kapteijn, F.; Hensen, E. J. M. Selective Coke Combustion by Oxygen Pulsing During Mo/ZSM-5-Catalyzed Methane Dehydroaromatization. *Angew. Chem. Int. Ed.* **2016**, *55* (48), 15086–15090. https://doi.org/10.1002/anie.201609442.

(214) Sily, P. D.; Noronha, F. B.; Passos, F. B. Methane Direct Conversion on Mo/ZSM-5 Catalysts Modified by Pd and Ru. *J. Nat. Gas Chem.* **2006**, *15* (2), 82–86. https://doi.org/10.1016/S1003-9953(06)60012-1.

(215) Aboul-Gheit, A. K.; Awadallah, A. E.; El-Kossy, S. M.; Mahmoud, A.-L. H. Effect of Pd or Ir on the Catalytic Performance of Mo/H-ZSM-5 during the Non-Oxidative Conversion of Natural Gas to Petrochemicals. *J. Nat. Gas Chem.* **2008**, *17* (4), 337–343. https://doi.org/10.1016/S1003-9953(09)60005-0.

(216) Aboul-Gheit, A. K.; Awadallah, A. E. Effect of Combining the Metals of Group VI Supported on H-ZSM-5 Zeolite as Catalysts for Non-Oxidative Conversion of Natural Gas to Petrochemicals. *J. Nat. Gas Chem.* **2009**, *18* (1), 71–77. https://doi.org/10.1016/S1003-9953(08)60080-8.

(217) Cheng, X.; Yan, P.; Zhang, X.; Yang, F.; Dai, C.; Li, D.; Ma, X.-X. Enhanced Methane Dehydroaromatization in the Presence of CO2 over Fe- and Mg-Modified Mo/ZSM-5. *Mol. Catal.* **2017**, *437*, 114–120. https://doi.org/10.1016/j.mcat.2017.05.011.

(218) Burns, S.; Hargreaves, J. S. J.; Pal, P.; Parida, K. M.; Parija, S. The Effect of Dopants on the Activity of MoO3/ZSM-5 Catalysts for the Dehydroaromatisation of Methane. *Catal. Today* **2006**, *114* (4), 383–387. https://doi.org/10.1016/j.cattod.2006.02.030.

(219) Liu, Z.; Nutt, M. A.; Iglesia, E. The Effects of CO2, CO and H2 Co-Reactants on Methane Reactions Catalyzed by Mo/H-ZSM-5. *Catal. Lett.* **2002**, *81* (3), 271–279. https://doi.org/10.1023/A:1016553828814.

(220) KojimaRyoichi; KikuchiSatoshi; IchikawaMasaru. Effects of Rhodium Addition to Mo/HZSM-5 Catalyst for Methane Dehydroaromatization. *Chem. Lett.* **2004**. https://doi.org/10.1246/cl.2004.1166.

(221) Kojima, R.; Kikuchi, S.; Ma, H.; Bai, J.; Ichikawa, M. Promotion Effects of Pt and Rh on Catalytic Performances of Mo/HZSM-5 and Mo/HMCM-22 in Selective Methane-to-Benzene Reaction. *Catal. Lett.* **2006**, *110* (1), 15–21. https://doi.org/10.1007/s10562-006-0087-x.

(222) Gnep, N. S.; Martin de Armando, M. L.; Guisnet, M. Toluene Disproportionation and Coke Formation over Fluorided Alumina and Hydrogen-Mordenite. *React. Kinet. Catal. Lett.* **1980**, *13* (3), 183–189. https://doi.org/10.1007/BF02068564.

(223) Gnep, N. S.; Martin de Armando, M. L.; Marcilly, C.; Ha, B. H.; Guisnet, M. Toluene Disproportionation and Coke Formation on Mordenites Effect of Catalyst Modifications and of Operating Conditions. In *Studies in Surface Science and Catalysis*; Delmon, B., Froment, G. F., Eds.; Catalyst Deactivation; Elsevier, 1980; Vol. 6, pp 79–89. https://doi.org/10.1016/S0167-2991(08)65221-0.

(224) Shu, Y.; Ichikawa, M. Catalytic Dehydrocondensation of Methane towards Benzene and Naphthalene on Transition Metal Supported Zeolite Catalysts: Templating Role of

Zeolite Micropores and Characterization of Active Metallic Sites. *Catal. Today* **2001**, *71* (1), 55–67. https://doi.org/10.1016/S0920-5861(01)00440-0.

(225) Yao, S.; Sun, C.; Li, J.; Huang, X.; Shen, W. A 13CO Isotopic Study on the CO Promotion Effect in Methane Dehydroaromatization Reaction over a Mo/HMCM-49 Catalyst. *J. Nat. Gas Chem.* **2010**, *19* (1), 1–5. https://doi.org/10.1016/S1003-9953(09)60031-1.

(226) Skutil, K.; Taniewski, M. Some Technological Aspects of Methane Aromatization (Direct and via Oxidative Coupling). *Fuel Process. Technol.* **2006**, *87* (6), 511–521. https://doi.org/10.1016/j.fuproc.2005.12.001.

(227) Liu, S.; Wang, L.; Ohnishi, R.; Lchikawa, M. Bifunctional Catalysis of Mo/HZSM-5 in the Dehydroaromatization of Methane with CO/CO2 to Benzene and Naphthalene. *Kinet. Catal.* **2000**, *41* (1), 132–144. https://doi.org/10.1007/BF02756152.

(228) Jahangiri, H.; Bennett, J.; Mahjoubi, P.; Wilson, K.; Gu, S. A Review of Advanced Catalyst Development for Fischer–Tropsch Synthesis of Hydrocarbons from Biomass Derived Syn-Gas. *Catal. Sci. Technol.* **2014**, *4* (8), 2210–2229. https://doi.org/10.1039/C4CY00327F.

(229) Kidnay, A. J.; Parrish, W. R.; McCartney, D. G. *Fundamentals of Natural Gas Processing*, 3rd ed.; CRC Press: Boca Raton, 2019. https://doi.org/10.1201/9780429464942.

(230) Otto, A.; Grube, T.; Schiebahn, S.; Stolten, D. Closing the Loop: Captured CO_2 as a Feedstock in the Chemical Industry. *Energy Environ. Sci.* **2015**, *8* (11), 3283–3297. https://doi.org/10.1039/C5EE02591E.

(231) Bedard, J.; Hong, D.-Y.; Bhan, A. Co-Processing CH 4 and Oxygenates on Mo/H-ZSM-5: 2. CH4 –CO2 and CH4-HCOOH Mixtures. *Phys. Chem. Chem. Phys.* **2013**, *15* (29), 12173–12179. https://doi.org/10.1039/C3CP50855B.

(232) Bedard, J.; Hong, D.-Y.; Bhan, A. C to H Effective Ratio as a Descriptor for Co-Processing Light Oxygenates and CH 4 on Mo/H-ZSM-5. *RSC Adv.* **2014**, *4* (90), 49446–49448. https://doi.org/10.1039/C4RA10661J.

(233) Tan, P. L.; Au, C. T.; Lai, S. Y. Effects of Acidification and Basification of Impregnating Solution on the Performance of Mo/HZSM-5 in Methane Aromatization. *Appl. Catal. A: Gen.* **2007**, *324*, 36–41. https://doi.org/10.1016/j.apcata.2007.03.002.

(234) Liu, S.; Ohnishi, R.; Ichikawa, M. Promotional Role of Water Added to Methane Feed on Catalytic Performance in the Methane Dehydroaromatization Reaction on Mo/HZSM-5 Catalyst. *J. Catal.* **2003**, *220* (1), 57–65. https://doi.org/10.1016/S0021-9517(03)00236-7.

(235) Ma, H.; Kojima, R.; Kikuchi, S.; Ichikawa, M. Effective Coke Removal in Methane to Benzene (MTB) Reaction on Mo/HZSM-5 Catalyst by H2 and H2O Co-Addition to Methane. *Catal. Lett.* **2005**, *104* (1–2), 63–66. https://doi.org/10.1007/s10562-005-7437-y.

(236) Benson, S. W. III - Bond Energies. *J. Chem. Educ.* **1965**, *42* (9), 502. https://doi.org/10.1021/ed042p502.

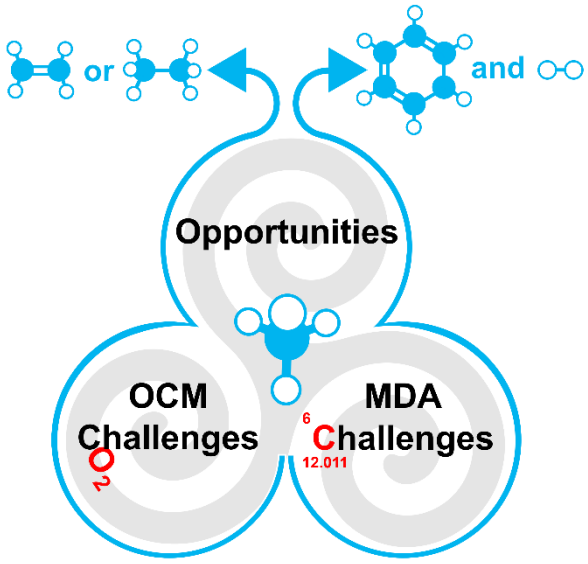

For Table of Contents Only